SANDIA REPORT

SAND2012-10744
Unlimited Release
Printed December 2012

Use of radial self-field geometry for intense pulsed ion beam generation above 6 MeV on Hermes III

Timothy J. Renk, Victor Harper-Slaboszewicz, Kenneth A. Mikkelson, W. Craig Ginn, Michael Schall and Gary W. Cooper

Prepared by
Sandia National Laboratories
Albuquerque, New Mexico 87185 and Livermore, California 94550

Sandia National Laboratories is a multi-program laboratory operated by Sandia Corporation,
a wholly owned subsidiary of Lockheed Martin company, for the U.S. Department of Energy's National Nuclear Security Administration under contract DE-AC04-94AL85000.

Approved for public release; further dissemination unlimited.

Issued by Sandia National Laboratories, operated for the United States Department of Energy by Sandia Corporation.

NOTICE: This report was prepared as an account of work sponsored by an agency of the United States Government. Neither the United States Government, nor any agency thereof, nor any of their employees, nor any of their contractors, subcontractors, or their employees, make any warranty, express or implied, or assume any legal liability or responsibility for the accuracy, completeness, or usefulness of any information, apparatus, product, or process disclosed, or represent that its use would not infringe privately owned rights. Reference herein to any specific commercial product, process, or service by trade name, trademark, manufacturer, or otherwise, does not necessarily constitute or imply its endorsement, recommendation, or favoring by the United States Government, any agency thereof, or any of their contractors or subcontractors. The views and opinions expressed herein do not necessarily state or reflect those of the United States Government, any agency thereof, or any of their contractors.

Printed in the United States of America. This report has been reproduced directly from the best available copy.

Available to DOE and DOE contractors from
U.S. Department of Energy
Office of Scientific and Technical Information
P.O. Box 62
Oak Ridge, TN 37831

Telephone: (865) 576-8401
Facsimile: (865) 576-5728
E-Mail: reports@adonis.osti.gov
Online ordering: http://www.osti.gov/bridge

Available to the public from
U.S. Department of Commerce
National Technical Information Service
5285 Port Royal Rd.
Springfield, VA 22161

Telephone: (800) 553-6847
Facsimile: (703) 605-6900
E-Mail: orders@ntis.fedworld.gov
Online order: http://www.ntis.gov/help/ordermethods.asp?loc=7-4-0#online

Use of radial self-field geometry for intense pulsed ion beam generation above 6 MeV on Hermes III

Timothy J. Renk
Electromagnetic Launch Systems
tjrenk@sandia.gov

V. Harper-Slaboszewicz and W. Craig Ginn
Radiation Effects Research

K. A. Mikkelson
Agt Accelerator Operations

Michael Schall and Gary W. Cooper
University of New Mexico
Albuquerque, NM 87131

Abstract

We investigate the generation and propagation of intense pulsed ion beams at the 6 MeV level and above using the Hermes III facility at Sandia National Laboratories. While high-power ion beams have previously been produced using Hermes III, we have conducted systematic studies of several ion diode geometries for the purpose of maximizing focused ion energy for a number of applications. A self-field axial-gap diode of the pinch reflex type and operated in positive polarity yielded beam power below predicted levels. This is ascribed both to power flow losses of unknown origin upstream of the diode load in Hermes positive polarity operation, and to anomalies in beam focusing in this configuration. A change to a radial self-field geometry and negative polarity operation resulted in greatly increased beam voltage (> 6 MeV) and estimated ion current. A comprehensive diagnostic set was developed to characterize beam performance, including both time-dependent and time-integrated measurements of local and total beam power. A substantial high-energy ion population was identified propagating in 'reverse' direction, i.e. from the back side of the anode in the electron beam dump. While significant progress was made in increasing beam power, further improvements in assessing the beam

focusing envelope will be required before ultimate ion generation efficiency with this geometry can be completely determined.

ACKNOWLEDGMENTS

The authors acknowledge the technical support of the Hermes facility staff – Gary Tilley, Chris Kirtley, and J. J. Montoya. The authors also acknowledge fruitful technical discussions with Paul Ottinger and Joseph Schumer of the Naval Research Laboratory, and Steve Rosenthal and Bryan Oliver of Sandia.

1. INTRODUCTION

Pulsed intense ion beams have been in development since the 1970s for a number of applications, among them materials processing [1-3], and beams as drivers for light ion fusion [4]. In the latter case, beam energies of 10 MeV and above were desired for maximizing energy delivered to an eventual fusion target [5,6]. For materials processing, energies < 1 MeV are typically used. We report here on experiments with the goal of generating focused intense ion beams on the Hermes III accelerator at Sandia National Laboratories. Hermes III (18 MV, 40 ns, 600 kA) is a 20-cavity multi-stage linear induction voltage accelerator (IVA) normally operated in negative polarity for the production of pulsed electron beams. It has been described in detail elsewhere [7,8]. Prior ion beam generation experiments were successfully conducted at up to 16 MV output voltage [8] with cavities configured for positive polarity operation. In those earlier experiments, the goal was impedance behavior characterization rather than focused ion beam power. Aspects of those experiments, and beam generation experiments at the 3-5 MeV level conducted on the Aurora pulser [9] (160 ns, 200 kA) and Mercury pulser [10] (50 ns, 325 kA) were reference points for the current set of ion beam experiments.

The key requirements of efficient ion beam generation are a) suppression of electron flow, and b) a high-current ion source. Electron suppression is necessary because, if high voltage is applied across a single stage anode-cathode (A-K) gap such as normally used for beam generation, two-species Child-Langmuir estimates [11,12] with protons as the ion species lead to only 2.3% of the current flow in ions. One method of electron suppression is the application of an external magnetic field, as in a magnetically insulated (MI) ion diode [13,14]. This requires additional capacitor banks with attendant complexity, and which for a > 5 MeV diode, a desired goal in these experiments, poses significant engineering challenges.

A simpler alternative is a ‘self-field’ design [15], in which the electron flow itself leads to suppression of the electron current component. This was the basis of the pinch-reflex ion diode [16] pioneered by the Naval Research Laboratory (NRL). Fig. 1 shows a schematic drawing of the NRL design for a focusing ion beam. This design was adapted for use in the initial Hermes experiments detailed here, and will be referred to as the ‘axial diode’ design. The diode is cylindrically symmetric about the extraction axis, with diode radius R and diode A-K gap D.

Electrons are emitted at large radius from a blade cathode and initially cross directly to the anode. As the diode current increases, however, there is a v x B force exerted in the radial direction on the electrons, bending their orbit so that they impinge on the anode surface at increasingly glancing angles. Behind the anode surface, a combination of electric and magnetic fields reflects the electrons back through the foil. If the anode material is thin enough (foil material), the electrons can reflex several times as they converge on the diode axis. The electron lifetime in the A-K gap thus increases roughly as R/D. This has led to demonstrated ion efficiencies (I_{ion}/I_{diode}) in low-impedance (e.g. low D/R ratio) diodes of as much as 50%, or ~ 20 times the Child-Langmuir ion current limit. The electron orbits result in heating of the anode foil which has the added benefit of providing a source of ions by 'turning on' the anode, i.e. supplying input energy to heat the foil constituents to vaporization and then ionization temperature. Ions are then extracted and propagate along the diode axis through the cathode region. Various forms of plastic foil have been used in such a diode, so that the foil composition is a mixture of hydrogen and carbon. Upon ionization, the proton component of the plasma, being of lighter mass than the carbon, is preferentially accelerated to form a proton beam. The carbon can be ionized to as much as +4 charge state, and so the total ion beam is composed of protons (~90% by number) and various charge states of carbon.

In the NRL experiments mentioned above, the forward-going power was delivered using a single-stage pulsed-power feed (2 Ohm output impedance) with inner and outer conductors. The Hermes output voltage is delivered to a coaxial magnetically insulated transmission line (MITL)[17] of 34 Ohm vacuum impedance ($=Z_o$). MITL operation is typified by electron emission from the negative coaxial conductor because the surface voltage exceeds the emission threshold. The electron flow, while initially lost to the positive conductor, results in a self-magnetic field that bends the subsequent emitted electrons downstream towards the diode load. This electron flow then constitutes a separate energy transport from that flowing in the metal conductors, and the behavior of this flow must be taken into account when matching the Hermes MITL to the diode load. In addition, since a direct measurement of either MITL or diode voltage is problematic in Hermes (and in IVA machines in general), voltage estimates derived from MITL theory provide an important prediction of voltage coming forward to the load.

While a full discussion of MITL dynamics is outside the scope of this paper, we address the implications of MITL operation into the ion diode in both positive and negative polarity, as discussed in the following sections. For our purposes here, the presence of vacuum electron flow alters the effective MITL impedance. The diode must operate closer to the MITL impedance for optimum energy transfer to the diode, and the result is that ion efficiency is reduced as the diode impedance is increased. Previous high-impedance experiments on the Aurora and Mercury pulsers, as mentioned above [9,10], were conducted at the 3-5 MeV level, and ion efficiencies on the order of 20% were observed. While the hardware dimensions were different, general aspects of those experiments resemble the current Hermes configuration enough so that ion efficiency on the order of 20% could be reasonably expected here also.

The initial Hermes MITL configuration was chosen to be positive polarity (i.e. the center conductor is pulsed to positive high voltage), in order to achieve convenient beam extraction from the diode hardware for diagnostic study. However, unlike the case in the prior Hermes full-power ion diode experiments, the cavities were left in their configuration for optimized operation in negative polarity, which is the dominant mode of Hermes operation. To avoid insulator flashover, the capacitor charging voltage was reduced with forward-going voltage designed to be half the normal 16 MV output (‘half-machine’). Because of this, and because of some unexpected power flow losses (described more below), output ion energy in positive polarity was typically 4 - 5 MeV. By reconfiguring the MITL hardware, another mode of operation was available that resulted in doubling of the power pulsewidth, at the same output voltage (‘long pulse’ mode). Long-pulse operation was restricted to a subset of shots, due to the added stress to machine hardware in this mode.

In order to investigate whether the power flow losses mentioned above could be mitigated by switching machine polarity, the final configuration investigated featured ion beam experiments in negative polarity (ion beam propagates into the machine. In this mode, (both standard and ‘long-pulse’), the power flow losses largely disappeared, and output rose to 6-8 MeV. Use of both positive and negative polarity configurations have led to implications for ion diode operation as the load for a MITL, as will be detailed in the experiment discussions below.

In considering the mating of the ion diodes described in this work to a MITL, several points need to be made: 1) the current that ultimately flows in the diode region will be some combination of the MITL vacuum flow that is incorporated into and becomes part of the current in the diode A-K gap, and the current generated by the diode operation itself, (i.e. the current emitted from the cathode tip plus the anode current once the ion source turns on). Ideally, optimum diode operation would result in as much of the flow current being incorporated as possible; and 2) behavior of the MITL in positive polarity is very different from negative polarity operation, and hence the interaction of the MITL with the diode load differs as well with polarity. The electron vacuum flow behavior in the two polarities is shown in Fig. 2, which is reprinted from Reference 10. This Figure depicts the results of LSP [18] simulations of MITL electron flow in the two polarities. In negative polarity operation (top), the electrons are born at the same potential, and follow orbits in a zone near the (negative) center MITL conductor. Many if not most of these electrons can be expected to flow into and become part of the diode current. In positive polarity, however, electrons emitted from the cathode of the successive adder cavities on the outer portion of the MITL are born at increasing potential with respect to their common anode as one moves from upstream (left- generator) to downstream (load) end. In this 'layered flow', electron orbits can occupy almost the entire volume on the interconductor MITL space, and many of these electrons could be lost to the diode current. The theory of electron behavior in negative polarity 'non-layered flow' has been developed by multiple researchers [19-22] and is relatively well understood. The most general form of the MITL voltage in negative polarity is taken from Ref. 22:

$$V = Z_o (I_A^2 - I_C^2)^{1/2} - \{g(V)m_e c^2/2e\} (I_A^2 - I_C^2)/ I_C^2 \qquad [1]$$

where Z_o is the MITL vacuum impedance, I_A and I_C are the anode-side and cathode-side currents, respectively, and g(V) is an adjustable parameter or order 1. The currents are measured at the same MITL axial position but on opposite sides, and well upstream of the diode load. For the Hermes negative polarity experiments, Z_o = 34 Ohms, and g ~ 0.8 [22].

Electron behavior in positive polarity with layered flow is complex, in particular because the layered flow involves turbulent behavior. Analysis of positive polarity systems with layered flow [23-25] has led to the conclusion that the MITL impedance is reduced compared to negative polarity. One estimate for MITL voltage in positive polarity with layered flow is given in Ref. 25:

$$V = (Z_o/2)\,(I_A^2 - I_C^2)^{1/2} \qquad [2]$$

Note that, if the second term is neglected in Eq. 1, Eq. 2 gives a factor of two lower estimate for MITL line voltage with layered flow compared to non-layered flow. That Hermes followed Eq. 2 scaling when operated at full power in positive polarity with layered flow was in fact the conclusion reached in the prior ion diode experiments [8]. Analysis of the present Hermes dataset discussed in Section 3 indicates that in these half-power experiments, Hermes tended to operate at a higher impedance in positive polarity than indicated by Eq. 2. This is one of the significant conclusions of the present work.

For planning of diode experiments, it is important to know the effective MITL impedance and its scaling behavior as a function of diode load impedance. In either polarity, the MITL impedance is best described by its flow impedance Z_f [26], which is a function of both the geometry and the voltage. The flow impedance is given by

$$Z_f = V/\,(I_A^2 - I_C^2)^{1/2} \qquad [3]$$

In the Hermes experiments, I_A and I_C are measured on a given shot. Equation 1 provides a set of MITL flow solutions in Z_oI_C - Z_oI_A space for a given voltage V. Such a plot is shown in Fig. 3, which is reprinted from Ref. 22. In this figure, the scaling factor g(V) has been incorporated from simulations [22]. For the left-hand edge of the voltage curves, $Z_f = Z_o/2$ (saturated flow), and for the right-hand edge, electrons flow very close to the cathode $I_c \sim I_a$ and $Z_f = Z_o$('super-insulated flow'). In the discussions in Section 3, the behavior of V(t) for various Hermes shots in this plot space will be described.

Before the power pulse reaches the diode load, the MITL will operate with a characteristic *self-limited impedance* Z_f^{SL}. The voltage and current generated at the diode load will depend upon the value of the load impedance Z_L compared to Z_f^{SL}. The load behavior will be largely determined by the diode characteristics if $Z_L < Z_f^{SL}$ ('load-limited'). The MITL characteristics will dominate if $Z_L \geq Z_f^{SL}$ ('line-limited'). For the voltages considered here, in non-layered flow (negative polarity), $Z_f^{SL} \sim 3Z_o/4$, and Z_f rapidly approaches Z_o as Z_L decreases below ~ $Z_f^{SL}/2$ [17]. In positive polarity with layered flow, however, Z_f^{SL} is normally expected to be closer to $Z_o/2$, and remains relatively low until till well into the load-limited regime. Thus, load impedance in positive polarity should generally be lower than in negative so as to avoid the 'line-limited' regime.

Section 2 describes the diagnostic suite that was developed over the course of the Hermes experiments that are described in Section 3. Initial experiments featured rudimentary diagnostics, and more were added in an attempt to more fully understand ion beam behavior. The structure of Section 4 reflects the evolution of the beam experiments from the initial axial pinch-reflex type diode (Fig. 1) operated in positive polarity to the final configuration of radial ion diode (described below) operated in negative polarity. We will focus on the latter configuration as by far the most successful in terms of beam power and focusing behavior. The positive polarity investigation, however, sheds some interesting light on the behavior of the Hermes MITL-diode combination, and some discussion will be devoted to this.

2. DIAGNOSTICS

2.1 Pulsed power current diagnostics

All configuration experiments were performed in the MITL geometry shown in Fig. 4, with accelerator current diagnostics were in the positions shown. At each IAS position (outer), 4 current shunts labeled IAS are arranged symmetrically around the inside of the outer conductor of the coaxial transmission line. In addition, 4 Bdot probes labeled MA are located at the same axial location on the outer conductor. The KBE are Bdot probes located around the outside of the inner conductor nearly opposite the IAS2 position. When possible, MITL voltage estimates

were derived from data from IAS2 and KBE monitors. In positive polarity, the total current I_A is measured by the KBE and MA (backup) monitors mentioned above, with the bound current I_C derived from the IAS current shunts.

For the shots in the axial ion diode geometry (Fig. 1), the IAS2 monitors were not fielded, and so IAS1 signals were used instead. For the vast majority of shots, the boundary current was observed to undergo a ~5% erosion from the upstream IAS1 to the downstream IAS3 position, although in some of the shot series, the magnitudes and waveshapes of the three IAS shunt sets were almost identical.

Estimates for the MITL line voltage were calculated using the current signals for each configuration shot series using both Eq. 1 for non-layered flow, and Eq. 2 for layered flow. These estimates were then compared to diode voltages derived from a) diode models for both the axial and radial ion diodes, and b) voltage estimates inferred from the nuclear diagnostics and film stack data (see below). Prior to each shot series, the individual current waveforms were normalized and time-tied using short-circuit shots, in which it is assumed that currents measured at all locations are identical. Some anomalies were noted with the various current waveforms on subsequent diode shots, depending upon the particular configuration.

The positive polarity experiments proved the most difficult to analyze. In a number of shots, the KBE waveforms exhibited large signal excursions and/or timing offsets compared to the IASs. At the time of these shots series, the only other inner conductor monitors available were the MK6 monitors. These are a set of four Bdots similar to the MA probes, but located on the inner conductor well upstream (~ 1 meter) of the KBE location. In the cases with the most severe such excursions, the MK6 signals were substituted in place of the KBEs. While in general, the cause of these excursions was ascribed to side-effects of high voltage operation (e.g. electrons striking the cable set behind the anode), in some instances, the signal excursions appeared to be caused by actual current variations. The KBE signals were observed to match the IAS3 signals during the initial current rise, then separate and then come together with the IAS3, then separate a second time. Calculations using Eqs. 1 and 2 then predict a double-humped voltage behavior. Since a) the KBE and IAS2 waveforms behaved identically with no

current separations on the short-circuit shots, b) the current inflections occurred on each of the four individual signals making up the KBE signal average, and 3) features on both or either of the Fcups or Rogowski waveforms (discussed below) appear correlated with the first or second voltage hump, we believe that such double-hump behavior occurs in positive polarity. In the negative polarity experiments, no double current separation was observed.

We note also that for many of the shots, the KBE and IAS2 signals rose together for 10-20 ns before separating, suggesting that the MITL did not turn on at first. Consequently, the voltage is not well known at the start of these shots. But it should be pointed out that in almost all cases where Fcup and Rogowski data were compared with the voltage estimates, no signals occurred on either diagnostic until current separation occurred between KBE and IAS2.

2.2 Rogowski coil for total (global) ion current

A Rogowski coil [27] is used to characterize the total ion current, as shown in a close-up view of the diode region shown in Fig. 5. It was in place for the positive polarity shots with diode diameter 12 cm, and for some of the negative polarity shots. The theory of Rogowski coil operation to determine ion current is as follows: the ion beam passes through a thin (2-6 μm) aluminized plastic foil. As the ions transit the foil, neutralizing electrons are drawn around the ion current monitor, with the Rogowski coil then actually measuring this replacement current to the foil. The foil placement with respect to the cathode tip is important for correct measurement of this replacement current. The foil plane should be recessed one or two A-K gap lengths [28] behind the cathode tip. If the foil is too close to the cathode tip (not recessed enough), significant electron emission from the foil occurs, and the Rogowski coil overstates the ion current because it also measures this additional electron current pulled from the foil. If the foil is recessed too far, the space charge of the ion beam can drag charge-neutralizing electrons from the AK gap to the foil. Any resulting electron current to the foil would cause the current probe to understate the ion current. The use of this signal depends on the diode electric field being shielded from the foil during the time of ion beam measurement. The calibration factor for the Rogowski coil was determined by the construction of the coil. On a number of

shots, a short circuit was made through the Rogowski coil, so the Rogowski should measure the same level as the total machine current. On these shots, the Rogowski current determined using the design calibration agreed well with the machine current monitors. In addition, several load shots were made of the foil plane in different positions, as discussed above. The measured ion current was observed to vary with foil plane placement. For the shots discussed below, the foil plane was placed 1-2 A-K gaps behind the cathode tip.

2.3 Faraday cups for local ion current

After the gas-filled transport configuration was eliminated in favor of vacuum ion propagation, it became possible to field Faraday cups (Fcups), which must be operated in vacuum. The Fcups were of two sizes, and both were constructed with permanent magnets, operated unbiased, and used to characterize the local ion current density. They were usually fielded behind the thin foil used for the Rogowski coil measurement. In addition, secondary electrons liberated by ion impingement are confined within the cup. A small Fcup featured a 1.5 mm aperture, and a larger Fcup contained a much stronger magnet and 3.2 mm aperture. One of the possible sources of Fcup measurement error is due to an intense beam impinging on the front surface and evolving enough gas or plasma from the front plate to cause 'hole-closure', e.g. such a gas or plasma interferes partially or totally with the incoming ion flux. This may lead to a sudden decrease in measured beam intensity. The subject of Fcup hole closure is a complicated one, and in particular any sudden decrease in indicated current density may also be caused, for example, by the oncoming beam either 'turning off' or changing its direction away from the Fcup aperture.

The small Fcups have been absolutely calibrated [29] by validating against a measured melt duration (Si surface melting measured by laser reflectometer) and 1-D heat flow modeling, at fluences up to 2 J/cm^2 (50 A/cm^2 peak current density typical). However, indicated current densities measured by these Fcups in the Hermes experiments have reached as high as 1.5 kA/cm^2 on some shots, a value significantly outside the validation zone. In the case of the latter reading, the Fcup signal was observed to terminate prematurely, a possible sign of hole closure. However, the same small Fcup was observed to track ion signals as high as 1 kA/cm^2

throughout the full power power, suggesting that hole closure does not occur up to 1 kA/cm^2. In addition, the larger Fcup, when fielded in proximity to the small Fcup, showed readings of the same magnitude as the small Fcup, again reinforcing this conclusion. (The large Fcup was not observed to measure any 1.5 kA/cm^2 peak current density signals, because due to its bulk, it was not fielded on axis where the biggest current densities were observed.)

2.4 Proton activation diagnostics for (time-integrated) local ion fluence

In addition to Fcups, a proton activation diagnostic was used to estimate local ion beam fluence [30]. This consisted of arrays of small canisters containing material to be activated by the beam and referred to as 'peppershakers'. The term peppershaker refers to the outward appearance of the canister, which consists of a cylinder with a small hole in the center of one end resembling a peppershaker. The hole allows the beam to enter and impinge on the activation material, and at the same time should trap any ablated material inside the canister. In practice, such canisters were interspersed with Faraday cups in the beam focal area. After a shot, the peppershakers were collected, and the activated material characterized off-line in a counting facility. The result was an estimate of beam fluence (in μC/cm^2) at a particular location. Since thick-target activation yields are voltage-dependent, a voltage (fixed in our case for convenience) must be assumed for a given shot in order to derive a beam fluence estimate. The value of the fixed voltage was estimated by self-consistently comparing with the other diagnostics.

The acceptance cone for the peppershakers is a key constraint, since ions incident from outside this cone will not strike the activation material. For the peppershakers used in this experiment, the half-angle of the acceptance cone is 22 degrees. If the microdivergence of the ion beam is large or the angle of incidence of the ion beam with respect to the axis of the peppershaker is large, the ion fluence determined from the activation diagnostic will underestimate the true ion fluence.

Activation material for peppershaker deployment was chosen from the following reactions:

1) ^{7}Li(p,n)^{7}Be. This reaction has a 1.8 MeV threshold and increases steadily with impinging ion energy. The residual ^{7}Be nucleus decays by electron capture with a 53-day half-life. The lithium is contained in Lithium Fluoride (LiF) disks.

2) Two reactions on target Ti nuclei. The first is ^{47}Ti(p,n)^{47}V which has a 3.8 MeV threshold, and the residual nucleus decays by γ emission with a 32.6 minute half-life. The ^{47}Ti nucleus has a 7.5% natural abundance.
3) The second Ti reaction is ^{48}Ti(p,n)^{48}V, with a 4.9 MeV threshold, the residual nucleus also decaying by γ emission with a 16-day half-life. The ^{48}Ti nucleus has a 73.7% natural abundance.

In practice, in intercomparisons with Fcup signals located next to peppershakers, there appeared to be some systematic discrepancies between fluence predicted by nuclear activation (using an externally determined average voltage), and those measured by the Fcups. For example, in the case of the ^{7}Li(p,n)^{7}Be reaction, inferred fluences from peppershakers were similar to readings from nearby Fcups, but only for estimated load voltages < 2.5 MeV. The inferred fluence deviated badly from Fcup values for energies > 3 MeV. This may be due to errors in yield (calibrated off-site), or errors in fielding. Despite this, the peppershaker dataset in general tended to support the relatively low peak current densities and delivered charge in μC/cm^2 indicated by the Fcups. The titanium peppershakers yielding activation counts based upon the ^{47}Ti(p,n)^{47}V reaction (3.8 MeV threshold) gave overall the most consistent comparison with Fcup readings. Unfortunately, as the load voltage rose with the more successful radial diode configuration, especially in negative polarity operation, increased nuclear activation led to extended radiological hold times before access to the diode hardware was possible after a given shot. Since the half-life of the ^{47}Ti(p,n)^{47}V reaction is only 32.6 minutes, the amount of residual activity became too low to measure after such extended wait times.

Fig. 6 shows a photograph of an array of Fcups and peppershakers after an ion beam generation experiment. The peppershakers are shown with open tops, because the activation material has been removed. Over time, and with the development of the stacked radiochromic pinhole camera for imaging ions (see below), the load voltage came to be estimated by comparing the various local diagnostics with Eqs. 1-2 and diode impedance estimates (below) for self-consistency.

2.5 Voltage Diagnostics (time-integrated) using stopping power of materials

Another estimate of the load voltage was obtained by measuring the electron and ion beam penetration through absorbing material, using radiochromic film to record the depth of penetration. The electron energy was characterized using layers of thin radiochromic film separated by aluminum. Insensitive film was used, with a threshold dose for a visible signal of about 4 J/g. The maximum depth of penetration was determined by the presence of a visible signal on the radiochromic film, and after correcting for the electron angle of incidence, this was converted to maximum electron energy by comparison with the CSDA (continuous slowing down approximation) range [31], and then confirmed using the ITS electron-photon transport code [32].

The ion energy was characterized using an Ion Pinhole Camera, depicted schematically in Fig. 11 below, and shown in exploded view in Fig. 7. The camera was mounted downstream of the cathode, at the same location as the Faraday cup and peppershaker array. Inside, a film stack consisting of multiple sheets of 47 μm-thick nylon radiochromic film (FWT-60) is positioned to image the anode through the entrance pinhole. As the ions penetrate the film stack, they lose an amount of energy determined by the stopping power of the film. The film darkening is quantitatively connected with ion dose in a given layer. The film response was calibrated by exposing the film to known doses at a Co-60 irradiation facility. The optical density of exposed and unexposed film was measured using a scanning microdensitometer in transmission and reflection using green and red filters. This allows the optical density to be converted to dose. The measured dose-depth profile can then be unfolded into incident proton fluence in different energy bins, using the response functions calculated from the Stopping Power of Ions in Matter (SRIM) program [33] and shown in Figure 8.

2.6 Witness Plate

On most shots the diagnostic array was protected by a 0.5 mm thick aluminum plate, with holes for the various diagnostics. Stainless steel witness plates were used on a few shots. The visible damage pattern on the plate characterized the ion beam size, and its position with respect to the different diagnostics. The spall layer thickness is approximately 0.1 mm. The fluence threshold for spallation is estimated using a spall threshold of 2.1 GPa for aluminum and 1.8 for stainless steel, stopping powers from NISTIR 4999 [31], and assuming instantaneous energy deposition with a Gruneisen coefficient of 2.25 for aluminum and 2.14

for stainless steel. The results are shown in Figure 9. At energies below the minimum energy on this plot, the ions do not penetrate 0.1 mm, and so cannot create a spall layer of that thickness. Hence, at lower energies, surface melting may be observed but a spall layer will not be observed.

2.7 Shadowbox

The position and direction of the ion beam was characterized using a "shadowbox" diagnostic as shown in Figure 10. The shadowbox is constructed by fabricating a set of radial aperture holes (forming ion beamlets) in a front plate capable of withstanding the full beam energy. A second blank plate is then mounted a short axial distance behind the front plate (2 cm in this case). By noting the damage marks on the back plate, and tracing the beamlet trajectories to the front plate aperture locations, the beamlet spot size as well as trajectory can be determined. In practice, this is accomplished by inserting thin rods through the apertures until they contact the respective damage spots on the witness plate.

3. EXPERIMENT SETUP

3.1 Positive polarity, axial pinch reflex diode (PRD)

Initial experiments were conducted in positive polarity with the axial focusing geometry shown in Figure 1. A focusing diode (curved) was followed by gas transport to 40 cm focal distance. The forward-going power in this configuration was significantly lower than predicted by modeling. We suspect that an upstream 'parallel load' was diverting considerable current from the downstream load. This may partly explain the beam generation and focusing that deviated from behavior observed in earlier NRL experiments with this diode. Shadowbox data indicated beam diverging away from the A-K gap in this configuration, not converging. The focusing diode was replaced by a flat geometry, and gas transport was dropped in favor of short beam transport in vacuum. The Kimfol membrane was left in place, and Fcups were added in the propagation region to measure local current density at various locations. Beam diagnostics indicated detection of relatively weak ion beam power persisting.

3.2 Positive Polarity, short-pulse mode, radial ion diode

In an attempt to improve beam power and address the diverging beam issue, the diode was changed from an axial to a radial design. Figure 11 gives a schematic view of the diode region with the radial diode hardware shown. The cathode tip projects from the outer MITL wall, and extends 2.5 cm along the axis with its downstream end flush with the anode plane. The 2.5 cm length was chosen so as to satisfy the length requirement [34] for the cathode to induce current pinching from the outer conductor for any ratio of inner to outer conductor likely to be fielded in these experiments. The anode itself is mounted at the end of a cylindrical tube.

Downstream of the cathode, the aluminized mylar that defines the Rogowski plane is fielded as before, at a distance of 6 cm from the anode. In comparing Fig. 11 with Fig. 1, it can be seen that the Rogowski foil in the radial diode geometry does not occupy the same 'recessed' position behind the cathode tip as is evident in Fig. 1. The discussion of Rogowski operation in Section 2.2 reflects NRL anecdotal findings using the Fig. 1 geometry, and comparable theory and experimental simulations of Rogowski behavior using the Fig. 11 geometry have not been attempted. Accordingly, interpretation of Rogowski data in the radial diode case may be problematic.

The drawing in Fig. 11 also depicts the Ion Pinhole Camera diagnostic at the downstream position, where the Fcups and peppershakers were also fielded. By the time of this experimental series, the Ion Pinhole Camera was routinely fielded in the diagnostics package, and thus voltage data were available for almost all of the shots in this series.

Simulations have been performed [35] which predict current flow with this geometry. When the power pulse arrives, electron emission begins uniformly along the cathode length. As the total current rises, electron orbits are bent by the increasing self-field until radial emission is cut off, and electrons are diverted downstream to the anode plane. The electrons then pinch radially inward towards the diode axis. This flow is predicted then to more uniformly 'turn on' the anode foil, compared to the diagonal electron flow inferred with the axial self-field diode (as will be discussed in Sec. 4.2.1). The length of the cathode along the diode axis is chosen so that enough electron current is emitted to initiate the orbit bending from the generated current self-field, i.e. to transition to the 'pinch'. This configuration change resulted in improved beam

focusing, as shadowbox data produced in the same manner as with the axial diode showed a converging ion beam.

3.3 Negative Polarity, short-pulse mode, radial ion diode

While the radial diode geometry yielded improved beam performance in positive polarity over that seen with the axial diode, total currents were still lower than what might be expected for the level of Hermes energy store. In order to investigate whether the positive polarity power flow results might be improved, the radial diode hardware was redesigned for fielding in negative polarity. A conceptual assembly drawing of the modified hardware is shown in Fig. 12. The anode tube is mounted on end of the MITL outer conductor to the left, and faces the cathode mounted on the Hermes III inner MITL conductor. The witness plate/diagnostics support is downstream (to the right) of the cathode, and contacts the cathode plate at large radius. Cabling for the Fcups and Rogowski extended through the Hermes center conductor. As previously mentioned, with the center conductor of the Hermes MITL charged negatively, all electron emission occurs at the same energy, and the electron flow in the MITL gap is restricted to a narrow region next to the inner conductor ('nonlayered flow'). Although negative polarity is considered an inconvenient ion generation mode (ion beam propagates into machine), this configuration was fielded with the goals of removing the upstream 'parallel load', and eliminating the 'layered flow'. Both total current and beam power were significantly improved.

3.4 Negative Polarity, long-pulse mode, radial ion diode

Hermes was operated in the 'long-pulse' mode as described above for several shots with the negative polarity radial ion diode. The resultant estimated ion beam energy exceeded 8 MeV, and total peak current increased from ~200 kA in the first axial diode shots to as high as 500 kA in this configuration. While diode current in long pulse mode increased significantly over short pulse mode, analysis of beam characteristics is incomplete due to the impingement and destruction of the principle beam diagnostics by the ion beam.

4. Results

4.1 Impedance behavior

4.1.1 Axial diode

From prior NRL work, the diode impedance Z_L for the axial pinch-reflex diode can be

estimated from the following formula [15, 36-37]:

$$Z_L \sim 36(D/R)[V/(1.022 + V)]^{1/2} \quad [4]$$

where D = A-K gap, R = diode radius, V = load voltage in MV, and 36 is an empirical factor that varies with D and V.

This formula was developed from experiments on the 2 Ohm non-IVA Gamble II generator, and for which D<<R. For these Hermes experiments, the MITL impedance is much higher, and D is on the same order as R. We assume that this formula is valid for use here, although the empirical factor may require alteration. In particular, an implicit assumption for IVA application is that some fraction of the electron flow current (e.g. difference between total and outer boundary current) is swept into the diode and adds to the diode current. However, for the case of 'line-limited' flow, i.e. where the diode impedance is on the order of the MITL flow impedance, it is reasonable to expect that a large fraction of the electron flow could be lost before it reaches the diode load. In this case, the empirical factor 36 may have to be reduced. For load-limited operation ($Z_L << Z_{FL}$), it is also reasonable to expect that the retrapping wave returning back from an undermatched load would result in much of the electron flow being incorporated into the diode current. Both assumptions ultimately need experimental verification, and in fact the Hermes data (below) suggests that even for relatively high diode impedance in this positive polarity mode, some fraction of the electron flow is incorporated into diode current. In case of the radial diode (Sections 3.2 – 3.3), the fraction appears to be considerable.

The A-K gap values fielded in this configuration varied from 1.2 to 5.2 cm, with anode radius varied between 6 and 3cm. We point out several of the shots in which an electron aluminum-radiochromic film stack was fielded to provide an independent measure of load voltage. On one of these (8287), taken with 5.2 cm A-K gap, analysis of the film stack resulted in a load voltage estimate of between 3.7 and 4.1 MV. Also on this shot, I_A and I_C (i.e. inner and outer MITL current) reached 185 kA and 134 kA, respectively. Using Eq. 2 and thus assuming fully-layered electron flow, as was observed in prior positive-polarity Hermes experiments, yields an estimate of 2.2 MV for the peak MITL voltage (Z_o = 34 Ohms). If instead, Eq. 1 is used with

both terms (assumes non-layered flow), the resulting voltage estimate is 4.1 MV. Thus it appears that electron flow in this geometry at this location is closer to non-layered than layered flow.

Switching now to a load impedance perspective, and assuming that Eq. 4 is valid, substituting the mid-point value of the radiochromic voltage estimate (3.9 MV) on Shot 8287 into Eq. 4 yields 27.8 Ohms for the load impedance. This implies that about 140 kA reaches the load, i.e. most of the electron vacuum flow appears to have been lost. Note that, aside from the Rogowski measure of ion current, a direct measurement of diode current is not possible in these experiments. Only the upstream total and bound currents are measured. If we assume then that all the electron MITL flow is lost, then the inferred voltage (Z_L x I_C) is 3.5 MV. If instead it is assumed that none of the total current is lost (181 kA), the upward bound for load voltage is 5.1 MV. If we assume non-layered flow and plot the trajectory of this shot on Fig. 3 in Fig. 13 by using $I_A(t)$ and $I_C(t)$, the trajectory is found to lie well to the right of the minimum-current flow line, and well away from the saturated (left-hand) side of the voltage contours. This is consistent with the non-layered flow conclusion reached above.

From another standpoint, using 3.9 MV as the voltage value from the radiochromic stack analysis, Eq. 4 can yield this voltage with 181 kA as the current used, but with the factor 36 reduced by ~25%, e.g. 27.9 instead of 36. This adhoc alteration of the empirical factor may be connected to a much different A-K gap aspect ratio from the NRL experiments, e.g. 5.2 cm A-K gap compared to the 6 cm diode radius. Using the 27.9 factor in Eq. 4 yields 21.5 Ohms for the load impedance estimate, which compared to the line impedance estimate of 34 Ohms implies that for this shot, the diode ran in the load-limited impedance regime. However, the assumption that almost all of the flow current is lost is more consistent with the 27.8 Ohm load impedance figure (relatively overmatched load). This implies that the factor 36 is more accurate than the lower 27.9 figure in Eq. 4.

This can be regarded as a heuristic approach to estimating diode behavior here, in the absence of other substantial voltage information with this shot series. As another example, we consider Shot 8493, which featured the same load geometry as Shot 8287 above, but was taken in 'long-

Pulse' mode with its much higher total current. Like Shot 8287, an electron radiochromic diagnostic was fielded along with an electron diode. On this shot, I_A and I_C = 290 kA and 133 kA, respectively. The radiochromic stack yielded a voltage estimate between 5.5 and 7 MV. The line voltage estimated from MITL theory (Eqs. 2 and 1, respectively) is 4.4 to 8.0 MV for layered and non-layered flow. If the factor 36 is again used in Eq. 4, with V = 6.25 MV (i.e., the average of the voltage measured by the radiochromic stack), the resulting diode impedance is 28.9 Ohms, roughly equal to that of Shot 8287 above. This gives a range of load voltage (when combined with I_C and I_A above) from 3.8 to 8.4 MV, the latter assuming that all of the 290 kA total current reaches the load. If we take the midpoint in the radiochromic voltage data as 6.25 MV, this gives a load current estimate of 216 kA, which suggests that relatively more of the flow current may be incorporated into the load on the long-pulse shot. The V(t) trajectory of this shot plotted on Fig. 3 is also shown in Fig. 13. The Shot 8493 trajectory starts (S) well into the insulated flow region, but then almost touches the minimum-current line before moving back to the right, ending up (F) to the left of the starting position. As for Shot 8287, its trajectory lies well to the right of the minimum-current flow line, but finishes closer to that line than where it begins.

The voltage and current estimates on the these shots with 5.2 cm A-K gap thus appear consistent with similar diode behavior in their respective short- and long-Pulse Hermes modes. What is more significant, however, is that the implied 3.9 MV voltage generated in the Short-pulse mode is only about half what Hermes normally produces with the same geometry in negative polarity. In addition, the 181 kA anode current is only a little more than half the 330 kA total current observed in negative polarity. While the reason for this discrepancy is unknown, it appears that there is a 'parallel load' upstream of the diode region that effectively diverts about half the current. Less current entering the diode region would be expected to affect diode operation, by in particular resulting in less current to the anode and delaying the ion 'turn-on'. This factor-of-two discrepancy with negative polarity is also inconsistent with LSP modeling [28] of the Hermes geometry in positive polarity. The lower-than-expected machine currents continued throughout the positive polarity experiments, and is one of the principal reasons for exploring diode operation in negative polarity.

The two above observations above – the output voltage scaling more consistently with non-layered (negative polarity) flow, and significant unexplained power losses upstream, may in fact be related [28]. It may be the case that the current loss results in most of the layered flow being shed upstream of the MITL position where the output voltage is calculated. In that case, the residual electron sheath may reside closer to the cathode, as occurs in negative polarity operation. That would explain why the downstream MITL behaves in a more non-layered fashion and hence a higher operating voltage than might otherwise be expected. This higher voltage, however, is gained at the cost of considerable upstream current loss. This change in operating point, if sustained in other IVA machines, has implications for future such experiments in positive polarity.

Since an A-K gap of 5.2 cm appears to result in near-line-dominated behavior, the A-K gap was lowered to 3.2 cm for a number of shots (8419-22) in an attempt to deliver more current to the load. The radiochromic film stack was not fielded for these shots. The impedance scaling indicated in Eq.4 is linear in A-K gap. Ignoring for the moment the possible effect of ion presence on the line impedance, scaling of the currents from Shot 8287 leads to a range of 1.8 MV (layered flow) – 3.6 MV (non-layered flow) MITL voltage for the shots with 3.2 cm A-K gap. Several of these shots featured LiF peppershakers, which for the $^{7}Li(p,n)^{7}Be$ reaction have a 1.8 MeV threshold and which showed significant activation, so that the load voltage must have been well above the layered flow value. Assuming a similar mid-point voltage operating point as Shot 8287, this implies a load voltage of ~2.7 MV for the 3.2 cm A-K gap shots, and load impedance of 12.6 Ohms. This implies that the 3.2 cm A-K gap shots ran in the load-limited regime, with an attendant decrease in diode voltage of at least 30%. The voltage loss seemed to offset any gain in diode current at this A-K gap, as anecdotal evidence (e.g. witness plate damage) continued to indicate weak beam power.

4.1.2 Positive Polarity Radial Diode

With the change to a radial A-K gap, the diode load impedance estimate of Eq. 4 no longer applies. One estimate of load impedance scaling can be obtained by scaling with a 'cylindrical diode' configuration [34, 35, 38]. In this geometry, an outer cathode protruding in at the end of the MITL provides converging electron current to the anode center conductor. The cylindrical

diode impedance scaling varies as ln (r_{outer}/r_{inner}), so that only the ratio of the radii influence the load impedance. Specifically, the diode impedance Z_d can be estimated from:

$$Z_d = 60/\alpha\ (\gamma_a\text{-}1/\gamma_a\text{+}1)^{1/2}\ \ln\ [r_{outer}/r_{inner}] \qquad [5]$$

where γ_a is the electron relativistic factor 1+ eV/mc^2, and α is a scaling factor connected to the level of pinching of the electron flow. The pinching level is determined principally by whether the electron flow to the anode side of the MITL results in ion 'turn-on'. If ions are not expected to be emitted from the positive side of the MITL, α is typically ~ 1.4 [35]. In the case of ion emission from the MITL anode surface, α increases to ~ 2.1 [34]. In the analysis below, it is seen that α ~ 1.4 leads to a more self-consistent agreement with voltage estimates from MITL theory and the stacked film voltage diagnostic. This implies no turn-on of ions in the radial gap, and while such a conclusion may be consistent with the large MITL dimensions (and hence relatively low specific energy deposition), it is also confirmed by simulations which show insufficient heating of the anode in the radial gap for turn-on in this geometry. On the other hand, the anode foil does turn on.

This formula was used to estimate the load impedance for both positive and negative polarity shots (below). In the latter case, of course, the outer conductor is at positive potential. For these estimates, the voltage was estimated self-consistently by comparing film stack measurements with MITL voltage calculated using Eqs. 1 and 2. The latter require inner and outer current behavior with time for a given shot.

Initial experiments were made with the radial diode geometry with different combinations of anode and cathode diameter. It was immediately apparent that centering of the anode with respect to the cathode was more important then with the axial diode, as might be expected. Adjustments were made to anode axis positioning until evidence of localized high current flow from the cathode side (e.g. arc marks and metal discoloration) appeared symmetric, along with beam vertical centering as indicated by witness plate damage. In addition, the spacing between the anode plane and plate holding the cathode was increased from 5 to 10 cm. Comparison of inferred voltage from shots where the 5 cm and 10 cm spacings were fielded indicate a lower

load voltage with the 5 cm spacing. This in turn implies that the anode stalk at larger radius than the anode ion source acts as a 'parallel load', effectively lowering the load impedance. The spacing was then fixed at 10 cm for the remainder of the Hermes III radial diode experiments.

The result of the inner-outer anode and cathode dimensional scan was that the best overall machine performance appeared to be with a radial A-K gap of 3 cm. This could be obtained with an inner anode diameter of either 6 or 8 cm, and cathode diameter of (respectively) 12 or 14 cm. Total load currents reached 170 kA, with typical Rogowski levels indicating 30 kA of ion current. The configuration with 6 cm and 12 cm for anode and cathode diameters, respectively (6-12), produced the highest inferred voltage, compared to the 8-14 configuration. This is consistent with Eq. 5 scaling, which predicts higher load impedance in the 6-12 case. Compared to the 8-14 configuration, the bound current in the 6-12 case (outer conductor IAS) dropped by ~ 10 kA.

Analysis of the 8-14 shots using Eq. 5 yields an estimate of 21.3 Ohms for the load impedance. For the 6-12 configuration, the estimate is 26.6 Ohms. Both cases assume $\alpha = 1.4$ and are approaching the 'line-limited' regime of load operation. Assuming the correctness of Eq. 5, these impedances are higher than for comparable shots in the axial diode dataset. For example, a 12 cm-diameter axial shot with 3.2 cm A-K gap (Section 4.1.1) operated at 12.6 Ohms impedance.

4.1.3 Negative polarity short pulse radial diode

LSP modeling for negative polarity operation similar to that performed in positive polarity predicted an increase in load current compared to the same radial diode geometry with a given A-K gap in positive polarity. This increase was realized, and discrepancy between modeling and experiment seen in positive polarity was greatly reduced. For example, the total current for the 8-14 radial diode configuration increased from 170 to 300 kA in negative polarity. Load voltage estimates increased significantly, both from the film stack data and from calculated voltage assuming non-layered vacuum flow (Eq. 1). In this shot series, typically ten layers of radiochromic film showed evidence of ion exposure, almost double the number typically seen

in positive polarity experiments. A comparison of load impedance and diode voltage between the two polarities can be seen in Fig. 14. (Eq. 5 was used to estimate the load impedance, with the inner and outer conductor dimensions simply switched between the two polarities.) Load impedance is observed to scale with ln [r_{outer}/r_{inner}] in both polarities, as predicted by Eq. 5. The impedance scales slightly higher for the same dimensions in negative polarity as compared to positive polarity. This is partly because, to better reconcile Eq. 5 scaling with voltage estimates, the empirical factor α was decreased from 1.4 to 1.2 in the negative polarity case. (Note that this again suggests that ions do not turn on in the radial gap of the diode.) The large difference in diode voltage between the two polarities is then caused not by a difference in load impedance, but by the large difference in total current between negative and positive polarity.

4.1.4 Negative polarity long pulse radial diode

A final series of three radial diode shots were taken in negative polarity, with Hermes III returned to the 'long-pulse configuration. Due to the longer power pulse, total load current increased from 300 to an impressive 500 kA. Calculated load voltages showed a slight increase (~0.5 MV) over the short-pulse beam shots, but the pulsewidth effectively doubled. This was confirmed by observed good agreement again in voltage waveshape to that inferred from the P-I-N diode diagnostic.

4.2 Ion beam behavior

4.2.1 Axial diode

There were two identified anomalies in beam operation during this axial ion diode series. In initial experiments with the focusing anode, witness plates were mounted at the beam focus shown in Fig. 1 (z = 40 cm). No damage was seen on the plates, even though Rogowski signals indicated ion beam currents of roughly 30-40 kA magnitude, an amount consistent with the ~20% expected ion efficiency mentioned above. Several shots were then taken with the witness plates moved closer towards the A-K gap. On one shot with a 3.2 cm A-K gap, the shadowbox diagnostic was fielded at a distance 10 cm from the A-K gap. The shadowbox result is shown in Fig. 10. In this photograph, the beam propagates downward from the top, and the rods mentioned previously are inserted through the apertures to contact the respective damage spots

caused. The rods appear pointed outward from normal, with the angle increasing with distance from the plate center. The beam reconstructed this way is clearly a diverging beam. Since the shadowbox front plate distance from the A-K gap is 10 cm, the tops of the rods shown in the photograph would roughly touch the anode surface were it to be installed. The divergence would appear to be caused by source behavior, as opposed to beam overfocusing. There is, however, an alternate explanation suggested by the prior Aurora experiments [9]. In those experiments, similar shadowbox fielding indicated that a) most ions appeared to come from the central region of the anode, and b) due to the electric field structure in the A-K gap, emitted ions from closest to the central axis appeared to be accelerated such that they cross the beam axis even in the A-K gap, whereas ions from further away from the axis were accelerated at similar angle but aimed to cross the axis further downstream. The net result then is that diverging ions were spread over the entire witness plate downstream of the A-K gap. Damage to the Hermes witness plates in fact shows that there is a consistent pattern of ion damage over a relatively large fraction of the witness plate area. This diverging beam character explains the lack of damage seen at 40 cm from the diode. But then the presumed ion paths shown in Fig. 1 (red lines) would be incorrect. In almost all of the subsequent shots taken after this series, both the curved anode and gas-filled transport were eliminated. The axial diode was eventually replaced in favor of the radial diode with the goal of modifying or eliminating the beam divergence behavior.

The second anomaly was an emerging discrepancy between the local beam diagnostics (Fcups and peppershakers) and the global ion beam measurement (Rogowski coil). In addition to witness plates, witness plate material made of flat 0.05 cm-thick aluminum was formed around the Fcup-peppershaker arrays fielded on various shots in all the configurations listed above. While areas indicative of beam impingement on the witness plate material typically covered 30-50 cm^2, the qualitative level of damage appeared slight and inconsistent with 30 – 40 kA of 4 MeV ions striking the thin aluminum surface. Furthermore, if the Rogowski signal is accurate, this suggests 50 – 100 $\mu C/cm^2$ striking the diagnostics. Initial activation measurements indicated proton fluences of at most 10 and as low as 0.05 $\mu C/cm^2$, assuming that the protons had the energy determined from the accelerator currents. Later Fcup measurements were also consistent with these low fluence values. While Fcup peak signals

approached 1 kA/cm^2 on some shots, these levels occurred in connection with smaller A-K gaps (and hence lower voltage). Furthermore, this level of current density was confined to the Fcup positioned on the center axis. At even a 2 cm distance off-axis, the peak level dropped by at least a factor 3.

This behavior is also similar to that observed in earlier experiments on the Aurora pulser [9], where an ion current density profile peaked on axis and a two component ion beam were observed. The ion beam had a 'pencil-like' forward-directed component on axis and a more diffuse strongly inwardly-directed component at larger radius. A possible explanation for this effect can be given by looking at Fig. 1. When D << R (leading to low diode impedance), initial electron emission proceeds directly across the A-K gap, followed by pinching towards the center as the electrons reflex through the anode foil on their way to the beam axis. However, when D ~ R, the presumed electron orbits follow a more diagonal path from their emission point towards the beam axis. The ion beam current density is then strongly peaked at central part of the anode, since the electron cloud at larger radius is kept away from the anode surface, and the outer component of the beam is accelerated inward by the electric field structure established by the diagonal electron flow pattern. This explains both the divergent ions on the witness plate, and the concentration of measured beam intensity on axis from the narrow forward-directed center of the beam. This ion beam behavior ultimately provided the motivation to transition to the radial diode geometry.

The local-global ion current discrepancy persisted through the radial diode experiments, and possible causes will be discussed in Section 4.2.2 below. (We have already mentioned the non-recessed position of the Rogowski foil as a possible cause.) This section details the change in diode hardware to that of a radial diode configuration.

4.2.2 Positive Polarity Radial Diode

In one of the 8-14 shots (8802), a full shadowbox with front plate made of 0.05 cm-thick stainless steel was fielded, replacing all of the local beam current diagnostics. The purpose was to compare the focusing behavior of the radial diode with that of the axial diode, as discussed

earlier. A photograph of the shadowbox front (head-on) taken after the shot is shown in Fig, 15a, and with rods inserted to trace the beamlet trajectories, as was done for the axial diode case (Fig. 10), in Fig. 15b. The shadowbox front indicates a centered melt pattern on the stainless steel. The rod positions imply a focusing beam originating from almost the entirety of the anode surface. This pattern differs dramatically from the diverging pattern seen in the axial diode case, and suggests that dynamics of the radial diode are quite different from the axial diode. Note that this finding does not mean that all the ions leaving the anode surface converged in the way shown, because the witness plate only records evidence of ions originating at the anode and which strike its surface with sufficient power to cause visible damage. As will be discussed below, there is evidence to support the idea that there are separate ion populations not being recorded by the shadowbox.

The damage to the stainless steel shadowbox front seen in Fig. 15a, along with damage seen on other ion shots, anecdotally points to increased ion beam power compared to the axial diode experiments. Part of this can be due to the higher ion energy, as mentioned above. The Fcup data for these radial diode shots, however, did not show increased magnitude compared to the axial shots, reaching only 220 A/cm^2 at most (Shot 8794), in a relatively narrow peak. The total charge delivered, based upon the Fcup waveform, was only 4.5 μC/cm^2, or significantly less than the best seen (30 μC/cm^2) on the 'diverging' axial diode shots. The front witness plate (made of 0.05 cm-thick aluminum) fielded for Shot 8794 can be seen after the experiment in Fig. 16. The three circular holes at large radius held the witness plate in position. The circular holes at smaller radii are through-holes for the ion beam to impact the various Fcups and peppershakers. As can be seen, the damage (defined by surface peeling outside the central holes) indicates a slightly off-center beam of ~15 cm^2 footprint. The Fcup recording the 220 A/cm^2 peak current was located behind the center hole. Note that the hole located in the southwest portion of the plate central area is outside the beam spall area. The Fcup located behind this hole showed only a small beam intensity. On a number of shots in the radial diode series, the beam footprint was small enough (and/or centered off-axis) that a number of the local diagnostic positions were outside the beam footprint.

A study of the signal waveforms for this series of shots, in which the anode and cathode

dimensions were varied, suggests more than one population of ions in the beam. This can be illustrated in Fig. 17, which shows waveforms from one of the 8-14 shots (8794). The plot shows a) total current (I_A) from the MK6 monitor, b) bound current (I_C) from IAS2, c) calculated voltage using Eq. 1 for non-layered vacuum flow (assuming any layered flow is lost upstream), d) Fcup signal from one of the small fielded Fcups, and e) Rogowski signal. The calculated voltage rises early in the power pulse, followed by a pause before continuing to its peak. The Fcup signal is observed to reach its peak value well before the voltage pause, whereas the Rogowski waveform shows only a slight 'foot' at the time of the Fcup rise (the Fcup and Rogowski signals are scaled to the others). The main part of the Rogowski signal, however, does not appear until the main peak of the calculated voltage. Both the Rogowski and voltage then decline together. The almost complete decoupling of Fcup and Rogowski waveforms could, among other possibilities discussed below, suggest that there are two ion populations, with only the earliest (and weakest) portion impinging upon the local current monitors. This would explain the low value of the Fcup signals despite the increased inferred ion beam power, but does not shed light on where the remainder of the ions measured by the Rogowski propagates.

Examination of other shots in this series shows similar implied two-component behavior. The effect occurs preferentially on the higher load impedance shots. In some cases, the voltage dip seen on Shot 8794 is more prominent, resulting in two discrete voltage spikes. In these cases, the Fcup waveform rises with the earlier pulse, and the Rogowski signal occurs primarily when the second voltage pulse rises.

Besides a two-component ion population, there are several other possible explanations for the discrepancy between the local and global ion beam measurements: 1) the Fcups and peppershakers are under-reporting the current; 2) the Rogowski coil calibration is incorrect; and 3) the beam propagates in a manner that results in some fraction of generated beam not reaching the position of the local diagnostics. While there is anecdotal evidence that the LiF peppershakers, in particular, underestimate the ion fluence above a beam energy of 2.5 MeV, the Fcups themselves, as previously indicated, have been observed to measure as high as 1 kA/cm^2 reliably. The peppershaker data from all three nuclear reactions, as it accumulated over

the series of shots, displayed complex behavior dependent upon the particular nuclear reaction studied, but in general tended to support the Fcup measurements, e.g. a low current density inconsistent with the measured total ion current as indicated by the Rogowski data.

We discuss two shots taken with the axial diode at small A-K gap as an illustration of a) the apparent ability of even the small Fcup to track current densities as high as 1 kA/cm^2, and b) internal consistency between Fcup and peppershaker data at voltages ~ 2.5 MeV or below. These shots were taken with reduced-diameter anode hardware, 6 cm instead of the 12 cm diameter shots discussed in Section 3.2. The diode performance at 6 cm anode diameter was similar to the larger diameter anode, except that the load impedance increased for the same A-K gap, as expected from the D/R scaling in Eq. 4. These shots in particular were taken with a different ion source, a thin-film titanium layer overcoated with palladium and loaded with hydrogen. The details of this ion source are discussed separately in the Appendix. On one of them (8524), the data from the Fcups and activation converged in an especially consistent manner. A schematic diagram of the fielding layout for this shot is shown in Fig. 18a. A small Fcup was mounted on the diode centerline, and another similar Fcup was mounted at a 2 cm radial distance from center. At the same radial distance, at different azimuthal positions were three peppershakers, two mounted with LiF target material and one with a titanium target. (The Ti peppershaker was not analyzed on this shot.)

The two LiF peppershakers located at the same radial distance from center gave identical activation counts. The Fcup waveforms from the shot are shown in Fig. 18b, along with a single Fcup signal from the previous shot (8523), taken with a plastic anode. The center Fcup recorded a peak current of 900 A/cm^2. The peak value is notable, but in addition the signal lasts the entire load voltage pulsewidth. The lack of premature cutoff or other anomalous features indicate that the small Fcup recorded current density properly at the 1 kA/cm^2 level. The Fcup located 2 cm off center reaches a much lower peak (125 A/cm^2), consistent with the center-peaked current density profile already mentioned. The center cup signal on the previous shot (8523 with plastic anode) reaches a 500A/cm^2 peak, but then exhibits an abrupt decline that could be caused by either source-limited cutoff, or a change to the local beam aiming behavior. The integrated charge from the two Fcups on Shot 8524 are 28 μC/cm^2 and 7 μC/cm^2 for the center and 2 cm-off center cups, respectively. The former value (along with 31 μC/cm^2 from the center cup on the second Ti/Pd shot, Shot 8525) represents the largest recorded charge of any of the axial diode shots. In addition, the 7 μC/cm^2 charge matches that implied by the two

LiF peppershakers, if an average load voltage of 2.5 MV is assumed. Applying Eqs. 1 and 2 to the three 1.2 cm A-K gap shots yields an average range of possible MITL voltage from ~ 1.6 to 3 MV. As noted previously, the 1.6 MV figure from the 'layered flow' mode must be too low, since appreciable activation from the LiF peppershakers (1.8 MeV threshold) occurred. Assuming the same effective MITL running impedance of $3Z_0/4$ as noted in the 6 cm radius anode discussion yields a voltage estimate of 2.4 MV, very close to that implied by the Fcup and activation diagnostics. If this value is inserted into Eq. 1 with the same 36 empirical factor used with the 6 cm-radius axial diode shots, this yields a load impedance estimate of 11.7 Ohms. Multiplying this value by the total current on Shot 8524 yields a load voltage estimate of 2.6 MV. Thus the voltage estimate from both MITL theory and the diode model agree with the voltage estimate from the nuclear diagnostics. The latter also agrees with the Faraday cup fluence estimate.

Finally, there is yet another possible source of unrecorded local ion current. The aluminized mylar used to define the Rogowski plane is at least one ion range thick for singly charged carbon ions at the beam energies estimated on the bulk of the Hermes shots. Prior NRL data point to a nontrivial carbon ion component to the beam generated from a plastic anode. For singly charged carbon, these ions would impinge on and be recorded at the Rogowski position, and be stopped within the mylar. Higher charge species would propagate through the foil. Estimates from Mercury ion experiments at NRL indicate that as much as 10% of the beam ions consists of carbon ions in various charge states, which would amount to about 15% of the total measured ion current using an average carbon state of +3 [9,10]. This would contribute to any discrepancy between local and total ion current measurements.

4.2.3 Negative Polarity Short Pulse Radial Diode

Beam operation in negative polarity was observed to differ in one significant way from that in positive polarity. The 'double-hump' behavior seen in radial diode shots in positive polarity did not occur in negative polarity. Calculated voltage from Eq. 1 was observed to rise in a broad smooth waveform. An additional diagnostic for the negative polarity shot series helped to confirm this voltage behavior. A P-I-N diode was fielded in a position to observe the general diode region. Since P-I-N signals scale as roughly $IV^{2.2}$, an estimate for the load voltage can be unfolded from the P-I-N signal using the total current (from the KBE monitors in this case). This unfold (scaled) is compared to the calculated load voltage from Eq. 1 for a 8-14 shot

(8842) in Fig. 19. This figure also shows the total current (I_A), bound current (I_C), and (scaled) large Fcup and Rogowski waveforms. Note the excellent waveform agreement between the two estimates of load voltage (i.e. apart from an overall scaling factor) with time, and the smooth separation of total and boundary current through the power pulse. Compared to the earlier positive polarity shots, the (large) Fcup and Rogowski signals behave similarly in time, but both appear delayed compared to the rise of the load voltage. The Rogowski signal reaches between 45 and 50 kA peak before it plateaus. The Fcup signal maximum is at 1 kA/cm^2 in a narrow peak, and is observed to apparently terminate prematurely (unlike the case with the small Fcup). The narrow pulsewidth results in a modest total integrated charge (only 10 μC/cm^2), which may be caused by a failure of the Fcup to track the high current density.

Despite the behavior of the Fcup in Fig. 19 (and typical of a number of these shots), there is qualitative evidence of significantly increased ion beam power over that seen in positive polarity as seen in the witness plates fielded for these shots. For example, in the axial diode shots in positive polarity, the surface of a 0.05 cm-thick Al witness plate typically showed a damage footprint and a peelback of the top surface layer of the aluminum. On Shot 8837 in this series, two such Al layers were mounted, one behind the other. A 3 cm-wide hole was blown through both plates from the incoming ion beam. On Shot 8839, a full shadowbox was fielded in similar fashion to Shot 8802 in positive polarity. A photograph of the shadowbox front plate (0.05 cm-thick stainless steel) is shown in Fig. 20a) before Shot 8839, and b) after the Shot. A photograph of the back of the Al witness plate mounted behind the front plate and taken after the shot can be seen in Fig. 20c. The front plate has a 2cm-wide hole blown through it, with pieces of the stainless steel bent backwards towards the Al witness plate. The witness plate shows the same damage, with pieces bent several cm out of the plane of the initially flat plate. While damage marks were also left by the beamlets propagating through the front shadowbox plate, the overall plate damage made it impossible to perform the ray-tracing to determine beam propagation behavior, as was done with the hardware after Shot 8802.

The peppershaker activation data yield generally lower estimates of delivered beam charges than the Fcups, sometimes much lower. Only on a single shot (8843) was an inferred charge as high as 15 μC/cm^2 delivered (LiF), although it should be noted that the peppershakers were

always mounted away from the beam axis by at least 2 cm. Also, the Rogowski signals for a number of these negative polarity shots appeared compromised, for instance showing early peaked behavior followed by large negative excursions. One possible cause is remnants of the ion beam impacting the signal cable located inside the center conductor. Accordingly, little usable data could be obtained from this diagnostic in negative polarity. The previously mentioned LSP simulations predict a ~ 75 kA total ion current for these negative polarity radial diode shots. The beam footprint indicated by the witness plate damage, plus the indicated charge delivery from the various diagnostics discussed above, do not together point to this much total current being measured, at least not to the focal area. Thus, there is still an apparent discrepancy between the local beam diagnostics and expected total current levels. Examination of the individual radiochromic films from a typical shot in this series (which image the anode surface) shows a number of 'hot spots' on the anode, i.e. locations whose size and position vary from shot to shot. Since the microdivergence and/or aiming position of beams emitted form these 'hot spots' is unknown, it is quite possible that a significant ion population crosses the Rogowski plane, but is not recorded by the local beam diagnostics.

Despite the problematic interpretation of the local and Rogowski current data, damage to the hardware as mentioned above, plus analysis of the power flow coming forward, both point to a substantial increase in both total and ion current generated in negative polarity with the radial diode. Consider one of the 8-14 negative polarity shots (8844). Total and bound currents I_A and I_C, respectively, reached 336 and 224 kA. These peak values are substantially higher than those attained with a similar 8-14 shot in positive polarity (8794 in Section 3.1). Those numbers were 200 and 160 kA, respectively. The Ion Pinhole Camera on Shot 8844 was heavily damaged by the oncoming ion beam, and the films inside were melted together. But similar 8-14 shots showed images on 10-12 films, indicating ion energies on the 8-14 shots of up to 8 MeV. The estimated MITL voltage on Shot 8844 (using Eq. 1) is 8.45 MV, although 7 MV is more typical in the other 8-14 shots. Using Eq. 5 with $\alpha = 1.4$ (Section 4.1.2) with V = 8.45 MV yields a load impedance estimate of 22.6 Ohms. Dividing this into the MITL voltage estimate gives a load current estimate of 374 kA. Since this is a higher value than the 336 kA measured total current, either the 8.45 MV estimate is too high, or Eq. 5 needs to be modified. If α is lowered to 1.3, the load impedance rises to 25.8 Ohms, yielding 336 kA as the load current.

Based upon the upstream total current measurement, this is as high as the load current could be. If instead, the estimated voltage is lowered to say 7 MV, this lowers the load impedance estimate from 22.6 to 22.3 Ohms and results in a 314 kA load current estimate. Given the general success in this investigation of the ability of MITL theory to predict forward-going voltage, it appears more likely that a slight change in the α factor from 1.4 to 1.3 better explains the data. In any case, this self-consistent analysis of a negative polarity radial diode shot suggests two clear conclusions of operation on Hermes: a) the anode side of the MITL does not 'turn on' in the radial diode gap in the course of the shot, and b) a relatively high proportion of the forward-going current is converted to diode flow in the radial diode, much higher than was indicated in the earlier case of positive polarity axial diode operation. The trajectory for this shot as plotted on Fig. 3 is shown in Fig. 21. It begins to the right of the minimum-voltage line, and progresses increasingly in the superinsulated direction as t increases.

Since no axial diode shots were taken in negative polarity, the question then is whether the inferred increase in the fraction of MITL current incorporated as load current in the radial diode case above is due to the change in polarity, or diode geometry. Since the radial diode was first operated in positive polarity, we consider one of those shots, Shot 8794. The configuration for the shot was also 8-14, and in addition, the Ion Pinhole Camera was undamaged and yielded a voltage estimate between 3.5 and 4 MV.

Returning to Eq. 5 and using $\alpha = 1.4$ as above and 3.75 MV for the voltage estimate, the estimated load impedance is 21.4 Ohms, and this combined with the total current (200 kA) yields a load voltage estimate of 4.3 MV. Increasing α to 1.5 results in a 20 Ohm and 4 MV load impedance and load voltage estimate, respectively. The MITL voltage estimate from Eq. 1 (using again ¾ Z_0) is 3.4 MV. Thus again, unless the load impedance estimate is incorrect, whether in positive or negative polarity, the radial diode as operated on Hermes III appears to incorporate the entire vacuum flow into load current. The trajectory for Shot 8794 (positive polarity), also plotted in Fig. 21, begins at the bottom right edge of the voltage contours (i.e. superinsulated edge) and ends slightly towards the minimum-voltage line, but still well in the insulated region.

One additional example is given by a lower load impedance shot from the short-pulse negative polarity series. This is Shot 8841, which featured a 12-16 configuration (2 cm radial A-K gap). Here, total and boundary currents I_A and I_C, respectively, reached 358 and 326 kA. The MITL voltage and load impedance estimates are 5.1 MV and 12.2 Ohms, respectively. The latter combined with total current yields a load voltage estimate of 4.4 MV. The trajectory for this shot (Fig. 22) traverses the far-right superinsulated zone. This is consistent with the well-insulated vacuum flow into an undermatched load.

In the course of the negative polarity radial diode experiments, another source of energetic ions was discovered and characterized by the local diagnostics. In the initial negative polarity beam experiment, the anode tube (left side in Fig. 12) was mounted initially with the same carbon beam stop that was fielded in positive polarity. After the shot, the beam stop was observed to be displaced away from the cathode and towards the vacuum end wall, made of 1.3 cm-thick aluminum. Significant damage was observed to the inside surface of the aluminum, in addition to spall damage on the outside surface. The damage was extensive enough to conclude that a vacuum breach nearly occurred. This points to a very energetic electron beam propagating away from the expected ion beam direction. On subsequent shots, in addition to the beam stop being reinforced, local beam diagnostics (Ion Pinhole camera, Fcups and peppershakers) were mounted in front of the beam stop for measuring ion current that may be co-moving with the intense electron beam, e.g. away from the cathode and towards the back of the anode tube. Such co-moving ions have been observed before [39]. On Shot 8845, identical assemblies of an Ion Pinhole Camera and one LiF peppershaker were mounted in opposite directions away from the A-K gap. The Radiochromic film stack in the two cameras recorded similar image sets. The activation count in the ‘backward’ direction was approximately half the level of that recorded in the normal ‘forward’ direction. On Shot 8847 (where both Ti and LiF peppershakers were mounted in the forward direction), the LiF peppershakers in the backward and forward direction were placed in slightly differing locations, but the relative count size was similar to Shot 8845. This suggests that the ion population co-moving with the high-energy electron flow into the anode represents about half the forward-going current. Informal calculations [28, 40] suggest that a virtual cathode is set up behind the anode plane due to electron penetration into

this area. Ions drawn in to neutralize the space charge can reach very high energies, well above the diode voltage. This would suggest that the ion population might be smaller than half the forward-going fluence, since the energies could be higher. While the ions here are not counted as part of the diode gap inventory, for applications where this ion population could be exploited (e.g. a secondary ion target behind the anode), the effective ion efficiency of the radial diode could be increased.
Further characterization of this high-energy ion population will be the subject of future work.

4.2.4 Negative Polarity Long Pulse Radial Diode

As already discussed in Section 3.4, due to the longer power pulse, total load current increased in the 'long-pulse' configuration from 300 to 500 kA, compared to short-pulse mode. Calculated load voltages showed an increase of ~1 MV over the short-pulse beam shots, but the pulsewidth effectively doubled. This was confirmed by observed good agreement again in voltage waveshape to that inferred from the P-I-N diode diagnostic. It is not clear, however, how much of this additional current was converted to useful ion beam. The Ion Pinhole Camera, which was mounted on the beam axis, was severely damaged by the apparently increased ion beam power, and the foil stack destroyed. The Fcups were mounted in the periphery of the expected beam to minimize damage. Their pulsewidth, although of ~ 50 ns duration, peak early in the current waveforms. Furthermore, when the Fcup signal peaks, there is a momentary pause in the total current on the rising part of the signal. The inner (bound) current also has an inflection point at this time, and increases thereafter rapidly to match the total current magnitude at current peak. This suggests a diode impedance collapse prior to the end of the power pulse. This could be caused by shorting of the A-K gap by plasmas evolved off of either the anode foil, or Rogowski foil, or both. Further evidence of this can be seen in the Z(t) waveform ($V_{Load}(t)/I_a(t)$) between Shot 8844 (short-pulse) and Shot 8957 (long-pulse). Both these shots featured the 8-14 configuration. The 8844 load impedance is fairly flat at ~ 25 Ohms through the power pulse. The 8957 load impedance is initially constant at 23 Ohms (i.e. slightly lower than 8844), but at the time the 8844 power pulse ends, the 8957 load impedance declines steadily till it is below 15 Ohms. During this time, the estimated MITL voltage (Eq. 1) remains above 9 MV, and the total current reaches 500 kA. On the V(t) trajectory curve (fig. 23), as the impedance falls, the path traced moves steadily up and to the right, almost leaving

the area covered by Fig. 3 completely.

The spacing between the anode and axial foil and diagnostics location may have to be increased in future experiments to prevent the evident gap closure indicated here.

Peak current magnitudes of the Fcup signal on the long-pulse shots reached 600 A/cm^2, less than that seen in the short-pulse shots. It is difficult to come to firm conclusions about diode behavior with such a small dataset, particularly when the main local beam diagnostics were damaged or destroyed on each shot. In addition to the goals for future work stated above, increased robustness of the diagnostics is required as well.

5. Summary and Conclusions

We have investigated the generation of high-power ion beams using the Hermes III facility, for the purpose of maximizing focused ion energy for a number of applications. Because of the need to alternate ion beam experiments with the more usual electron beam experiments on Hermes, the output voltage was restricted so as to not damage the Hermes IVA induction cavities. A self-field diode was chosen initially of the axial pinch-reflex type used on prior NRL beam formation experiments. Several diode designs were fabricated and tested, both in positive polarity (convenient beam extraction) and negative polarity (maximizes forward-going current). As each design was tested and modified, the indicated ion beam power increased. The diagnostic set was continually improved in order to characterize the ion beam. The final configuration tested, that of a radial diode operated in negative polarity 'long-pulse' mode, resulted in output voltages well above 6 MeV and total currents of up to 500 kA. This beam was characterized with a comprehensive diagnostic set including inner and outer current monitors, radiochromic film stack, P-I-N diode, and global (Rogowski) and local (Fcups and peppershakers) ion current monitors. While the ion beam was clearly substantially increased from beginning to end of the experiments, an estimate of total ion current proved challenging, as has been discussed above. Further, variations in hardware parameters undertaken in order to improve beam power, including changes in A-K gap, reduction of anode diameter from 12 cm, the size used for the bulk of beam experiments, to 6 cm, and lengthening of the power pulse

width by making use of the Hermes 'long pulse' mode, resulted in an extensive dataset of beam characterization as a function of diode design, A-K gap, anode diameter, etc.

The variation in A-K gap followed a predictable load line, e.g. higher indicated voltage and lower total current for the larger A-K gaps. In positive polarity, the output voltage did not follow the expected $Z_o/2$ behavior that typifies fully saturated vacuum flow, but rather seemed to follow the $3Z_o/4$ behavior expected of operation in negative polarity. This may be connected to the upstream loss which may have led to the shedding of most of the 'layered' flow, leading to current behavior more like that seen in operation with non-layered flow. Thus while output voltage in positive polarity appears to be higher than that expected for layered flow operation, current reaching the diode appears to be lower as well.

The discrepancy between local and global ion beam measurements was the subject of systematic investigation. The array of local diagnostics occupies only the central part of the region downstream of the cathode tip. It is possible that a portion of the ion beam could cross the aluminized mylar foil plane and be recorded by the Rogowski monitor, but not be observed by the Fcups, peppershaker arrays, or Ion Pinhole Cameras. Given that the original axial focusing geometry did not yield the expected beam behavior, this result would not be surprising. An additional source of discrepancy is that singly-charged carbon ions of the energies generated here will be stopped in the mylar, and hence could be recorded by the Rogowksi but not propagate to the local diagnostic location. Determining the exact beam aiming and propagation behavior is an incomplete aspect of the current work, and should be the subject of future experiments. There is also clear evidence of a 'reverse' population of energetic ions behind the anode emission area, which could be exploited in certain applications.

In order to obtain a more uniform ion beam, the axial diode was replaced by a radial diode design, where the pinching electron beam is expected to 'turn-on' a larger fraction of the anode area. Radial diode performance represented an significant improvement over axial diode performance. The most compelling difference was the confirmation of a focusing beam as indicated by ray-tracing using the shadowbox assembly. The ion beam energy increased over

that seen in axial diode experiments for the same A-K gap. As indicated by power flow calculations and validated by the V(t) trajectories in Fig. 3, almost all of the MITL total current became incorporated into load current. The witness plates showed increased beam damage. The Fcup and peppershaker signals, however, did not show an increase consistent with the increased damage seen on the witness plates. There is evidence from waveform data that in positive polarity, the Fcup and Rogowski signals respond to different ion populations. It is clear from examining a number of the Fcup and Rogowski signals, specifically correlations in waveform shape and timing, that overall the signals represent physical processes, and are not artifacts. In particular, the Fcups may underrepresent the ion beam local magnitude, but do not exhibit any overt signs of hole closure or other anomalous behavior.

In the transition from positive to negative polarity radial diode operation, diode performance was observed to improve significantly. Total diode current increased from 170 to 300 kA, for instance. The ion beam created 10 cm^2-area holes in two layers of 0.05 cm aluminum, and similar holes in 0.05 cm stainless steel followed by 0.05 cm aluminum plate (shadowbox assembly). Up to 10 layers of radiochromic film consistently showed exposure to ions in the Ion Pinhole camera, indicating a population of ions with energies exceeding 6 MeV.

A short campaign of 3 shots was taken in negative polarity, and with the short-pulse mode replaced by long-pulse Hermes operation. While total current increased by 50%, to 500 kA, it is not clear how much of this additional total current was converted to useful ion power. The ultimate ion beam power, while anecdotally increased from the short-pulse shots, is not known, since the Ion Pinhole cameras, Fcups and peppershakers located in the center of the beam footprint were completely destroyed. Fcups located outside the main beam focus showed only ~ 300 A/cm^2 peak current density. It is clear then future operation in this mode requires significantly increased diagnostic durability. That conclusion is notable in itself demonstrating the progress made in these Hermes ion beam experiments.

Appendix. Ion production from hydrogen-loaded titanium foils

The anode foil material used in the experiment series above consisted of several different types of plastic: 1) glycol-modified polyethylene terephthalate (abbreviated as PETG), and 2) polyvinyl acetate (PVA). Each is a complex hydrocarbon made of differing percentages of hydrogen and carbon. The PETG was chosen because it can be readily heat-formed into the curved shape initially used in the Hermes axial diode experiments. The PVA material is used as an ion source for ion beams generated at NRL. As mentioned previously, it is assumed that when sufficient electron energy is deposited in this material to raise it to vaporization and ionization temperature, that the lighter hydrogen is preferentially accelerated by the power pulse, and the resulting beam is composed predominantly of protons. As mentioned previously, prior NRL experiments point to a minority population of as much as 10% carbon ions, which would amount to about 15% of the measured ion current. What is not clear, and has not been investigated, is the timescale for ionic evolution from such plastic material.

We investigated an alternative to plastic anode material, in the form of hydrogen that has been absorbed by a thin titanium film. Titanium is well known as a getter, and hydrogen can be taken up and stored interstitially within the titanium lattice at up to 50 at%. Furthermore, it was hoped that heating of this layer may allow for faster evolution of the stored hydrogen to gaseous phase, compared to vaporizing and ionizing the hydrogen bound up in organic molecules. This might reduce the observed ~20 ns turn-on delay for ion beam production in the diode experiments discussed here. This kind of source was developed by the ion beam group at FZ Karlsruhe in the 1980s [41]. In the earlier work, a thin layer (500 Å) of titanium was sputter-deposited in-situ on a glass substrate. This was followed by an even thinner 200Å layer of palladium (Pd), whose purpose was to passivate the titanium, i.e. protect it from oxidizing. Then hydrogen gas is used to backfill the chamber to ~ 1 bar for 30 minutes. The hydrogen readily diffuses through the Pd layer (Pd was used in Cold Fusion experiments because of this property), and loaded into the Ti layer underneath. In the German experiments, an external pulser was used to heat the Ti film layer prior to the arrival of the machine power pulse.

For the current experiments, we did not plan to use an external pulser, and so we made an estimation of the appropriate materials and thicknesses. The glass was replaced with the titanium foil as a substrate, and the Ti and Pd layers were deposited by high-power ion beam

ablation using the RHEPP-1 facility [2]. The hydrogen was loaded by backfilling the RHEPP vacuum chamber to 350 Torr for approximately 40 minutes after the in-situ deposition. The estimated film thicknesses were 130 nm and 50 nm for the Ti and Pd layers, respectively. Later sample foil heating measurements using a separate vacuum chamber with a Residual Gas Analyzer (RGA) confirmed that hydrogen gas was released upon heating, although the time scale of this release is much slower than would occur on a Hermes shot. Separate experiments with deuterium gas loading confirmed that hydrogen is released in that case also. That hydrogen is presumed to be released from the Ti foil itself, since titanium is known to attract hydrogen, and is in fact used as gettering material.

During the axial diode experiments, two shots using this hydrogen-loaded film were taken, with an additional comparison shot taken using the a flat PETG foil, all with 2 cm nominal (1.2 cm actual) A-K gap. These shots were referred to in Section 4 above. The two hydrogen-loaded film shots displayed much higher Fcup current densities and longer pulsewidths than that seen one the shot with the PETG foil. The Faraday cup signal with the first plastic anode peaked at 400 and 500 A/cm^2 for the two Fcups used. For the next shots, the hydrogen-loaded Ti film produced 900 to 950 A/cm^2 peak. Thus the ion current measured at the beam center was increased significantly. The ion turn-on was delayed, however, by as much as 20 ns, and at a radius of 2 cm (the location of the other Faraday cup on the shots), the ion current dropped to 300 A/cm^2 peak.

While the ion output was increased with H-loaded Ti film anode, increased damage occurred to the anode film holder. This is attributed to the increased turn-on delay time. Several additional shots were taken with the H-loaded anode foil in the radial diode experiment series. In the latter case, the increased ion output compared to a plastic anode was not duplicated, but the longer ion turn-on delay occurred. In addition, data from multiple LiF arrays confirmed that ion current density varied across the beam footprint more than was seen in the axial diode case. Thus, the result of the H-loaded anode foil use produced mixed results. Improved results may be expected with the use of an external pulser to heat the film prior to the arrival of the power pulse, as used in the earlier German experiments. In addition, the use of a titanium foil backing complicates the experiment, as the foil itself can store hydrogen apart from that loaded into the

Ti thin film on top of the foil. The titanium foil was replaced with aluminum, and deuterium was successfully loaded into the Ti thin film (as confirmed by heating tests and RGS measurements), but the radial diode experiment ended before the Al film-backed source could be used to generate an ion beam. Use of the aluminum foil could possibly result in formation of a pure deuterium beam.

ACKNOWLEDGMENTS

The authors acknowledge the technical support of the Hermes facility staff – Gary Tilley, Chris Kirtley, and J. J. Montoya. The authors also acknowledge fruitful technical discussions with Paul Ottinger and Joseph Schumer of the Naval Research Laboratory, and Steve Rosenthal and Bryan Oliver of Sandia.

REFERENCES

1. A. D. Pogrebnyak, *Metastable states and structural phase changes in metals and alloys exposed to high power pulsed ion beams*, *Phys. Status Solidi (A)* **117** (1990) 17–51.
2. T. J. Renk, P. P. Provencio, S. V. Prasad, A. S. Shlapakovski, A. V. Petrov, K. Yatsui, W. Jiang, and H. Suematsu, *Materials Modification Using Intense Ion Beams*, Proc. of the IEEE **92** (2004) 1057-1081. Both this and Reference 1 have extensive bibliographies.
3. J. Piekoszewski, Z. Werner, W. Szymczyk, *Application of high intensity pulsed ion and plasma beams in modification of materials*, Vacuum **63** (2001) 475-481.
4. J. P. VanDevender and D. L. Cook, *Inertial Confinement Fusion with light ion beams*, *Science* **232** (1986) 831-836.
5. D. J. Johnson *et al.*, *Lithium beam generation and focusing with a radial diode on PBFAII*, *Laser Part. Beams* **16** (1998) 185–224.
6. T. J. Renk, G. C. Tisone, R. G. Adams, D. J. Johnson, C. L. Ruiz, and G. W. Cooper, *Development of the laser evaporation ion source for lithium beam ion generation on the Particle Beam Fusion Accelerator (PBFA-II)*, Physics of Plasmas **6** (1999) 3697.
7. R.C. Pate, J.C. Patterson, M.C. Dowdican, J.J. Ramirez, D.E. Hasti, K.M. Tolk, J.W. Poukey, L.X. Schneider, S.E. Rosenthal, T.W.L. Sanford, J.A. Alexander, and C.E. Heath, *Self-Magnetically Insulated Transmission Line (MITL) System Design for the 20-Stage Hermes-III Accelerator*, in the Proceedings of the 6th IEEE Pulsed Power Conference (Arlington, VA., June 1987) 478.
8. D. L. Johnson, J.A. Alexander, J.J. Ramirez, J.P. Corley, G.J. Denison, J.W. Poukey, T.R. Lockner, S.E. Rosenthal, and C. Ruiz, *Hermes-III Positive Polarity Experiment*, 7th IEEE Pulsed Power Conference, (Monterey, CA, 11-14 June 1989) 32.
9. R. A. Meger, F. C. Young, A. T. Drobot, G. Cooperstein, S. A. Goldstein, D. Mosher, S. E. Graybill, G. A. Huttlin, K. G. Kerris, and A. G. Stewart, *High-impedance ion diode experiments on the Aurora pulser*, J. Appl. Phys. **10** (1981) 6084-6093.
10. D. D. Hinshelwood *et al, Ion diode performance on a positive polarity inductive voltage adder with layered magnetically insulated transmission line flow*, Phys. Plasmas **18** (2011) 053106.
11. C. D. Child, *Discharge from CaO*, *Phys. Rev.* **32** (1911) 492–511.

12. I. Langmuir, *The effect of space charge and residual gasses on thermionic currents in high vacuum*, *Phys. Rev.* **2** (1913) 450–486.
13. R. N. Sudan and R. V. Lovelace, *Generation of intense ion beams in pulsed diodes*, *Phys. Rev. Lett.* **31**, no. 19 (1973) 1174–1177.
14. P. Drieke, C. Eichenberger, S. Humphries, and R. Sudan, *Production of intense proton fluxes in a magnetically insulated diode*, J. Appl. Phys. **47** (1976) 85-87.
15. Stanley Humphries Jr., *Self-Magnetic Insulation of Pulsed Ion Diodes*, Plas. Phys 19 (1977) 399-406.
16. S. J. Stephanakis, D. Mosher, G. Cooperstein, S. A. Goldstein, and J. R. Boller, *Production of intense proton beams in pinched-electron-beam diodes*, Phys. Rev. Lett. **37** (1976) 1543–1546.
17. J.P. VanDevender, J.T. Crow, B.G. Epstein, D.H. McDaniel, C.W. Mendel, E.L. Neau, J.W. Poukey, J.P. Quintenz, D.B. Seidel, and R.W. Stinnett, Physica **104C** (1981) 167.
18. LSP is a software product of ATK Mission Research, Albuquerque, NM 87110.
19. J.M. Creedon, *Relativistic flow in the high ν/γ diode*, J. Appl. Phys. 46 (1975) 2946-55.
20. C. W. Mendel, D. B. Seidel, and S. A. Slutz, *A general theory of magnetically insulated electron flow*, Phys. Fluids **26** (1983) 3628-35.
21. C. W. Mendel, D. B. Seidel, and S. E. Rosenthal, Laser Part. Beams **1** (1983) 311.
22. P.F. Ottinger and J.W. Schumer, *Rescaling of equilibrium magnetically insulated flow theory based on results from particle-in-cell simulations*, Phys. Plasmas **13**, 063109 (2006).
23. C. W. Mendel, Jr. and S. E. Rosenthal, *Modeling magnetically insulated devices using flow impedance*, Phys. Plasmas **2** (1995) 1332-42.
24. C. W. Mendel, Jr. and S. E. Rosenthal, *Dynamic modeling of magnetically insulated transmission line systems*, Phys. Plasmas **3** (1996) 4207-4219.
25. S. E. Rosenthal, *Characterization of Electron Flow in Negative- and Positive-Polarity Linear Induction Accelerators*, IEEE Trans. Plas. Sci **19** (1991) 822-830.
26. C. W. Mendel, *Planar one-dimensional magnetically insulated electron flow for arbitrary canonical-momentum distribution*, J. Appl. Phys. **50** (1979) 3830-7.
27. W. Rogowski and W. Steinhaus, *Die Messung der magnetischen Spannung*, Archiv fur Elektrotechnik **1** (1912) 141-150.
28. P. F. Ottinger, private conversation.

29. M. O. Thompson and T. J. Renk*, Numerical modeling and experimental measurements of pulsed ion beam surface treatment*, Mat. Res. Soc. Symp. Proc. **504**, 33 (1998).

30. Ruiz, C.L., Cooper, G.W., Chambers, G., and Schmidlapp, F.A., *Calibration of direct nuclear activation diagnostics for measuring intense proton, lithium, and fluorine beams*, Rev. Sci. Instrum. **68** (1997) 348.

31. Berger, M.J., Coursey, J.S., Zucker, M.A., and Chang, J. (2005), *ESTAR, PSTAR, and ASTAR: Computer Programs for Calculating Stopping-Power and Range Tables for Electrons, Protons, and Helium Ions* (version 1.2.3). [Online] Available: http://physics.nist.gov/Star [*20110325*]. National Institute of Standards and Technology, Gaithersburg, MD. Originally published as: Berger, M.J., NISTIR 4999, National Institute of Standards and Technology, Gaithersburg, MD (1993).

32. B. C. Franke, R. P. Kensek, T. W. Laub, and M. J. Crawford, "ITS Version 6: The Integrated TIGER Series of Coupled Electron/Photon Monte Carlo Transport Codes", Sandia National Laboratories Report **SAND2008-3331** (2009).

33. SRIM information can be obtained from http://www.srim.org. Reference for the companion TRIM code is: J. P. Biersack, J. F. Zeigler, Transport of Ions in Matter, IBM Research, Yorktown Heights, NY, 1995.

34. C. Cooperstein *et al*, Phys. Plasmas **8** (2001) 4618-4636.

35. S. B. Swanekamp, R. J. Commisso, G. Cooperstein, P. F. Ottinger, and J. W. Schumer, *Particle-in-cell simulations of high-power cylindrical electron beam diodes*, Phys. Plasmas 7 (2000) 5214 – 5222.

36. G. Cooperstein and J.J. Condon, J. of Appl. Phys. **46**, 1535 (1975).

37. S.J. Stephanakis, J.R. Boller, G. Cooperstein, J.C. Kellogg, B.V. Weber, and F.C. Young, Proceedings of the 9th International Conference on High-Power Particle Beams, Washington, DC, 1992, edited by D. Mosher and G. Cooperstein, (NTIS PB92-206168, Springfield, VA 1992), p. 871.

38. B. V. Oliver, P. F. Ottinger, T. C. Genoni, J. W. Schumer, B. Strasburg, S. B. Swanekamp, and G. Cooperstein, *Magnetically insulated electron flow with ions with application to the rod-pinch diode*, Phys. Plasmas 11 (2004) 3976-3991.

39. Graybill and J.R. Uglum, *Observation of Energetic Ions from a Beam-Generated Plasma*, J. Appl. Phys. **41**, 236 (1970).

40. P. F. Ottinger *et al*, *Acceleration of ions by an electron beam injected into a closed conducting cavity,* submitted for publication in Physics of Plasmas.

41. H. Bluhm et al, "Formation of a Homogeneous Hydrogen Plasma Layer for the Production of Terawatt Ion Beams," IEEE Tran. Plasma Sci. **21**, 560 (1993).

DISTRIBUTION

4 Lawrence Livermore National Laboratory
Attn: N. Dunipace (1)
P.O. Box 808, MS L-795
Livermore, CA 94551-0808

1	MS1179	Leonard Lorence	Org. 1341
2	MS1159	Victor Harper-Slaboszewicz	Org. 1344
1	MS1164	David L. Keese	Org. 5400
1	MS1179	Mark A. Hedemann	Org. 1340
1	MS1173	Vance L. Behr	Org. 5440
1	MS1182	Ronald J. Kaye	Org. 5445
1	MS1181	Larry X. Schneider	Org. 1650
5	MS1182	Timothy J. Renk	Org. 5445
1	MS1193	Michael E. Cuneo	Org. 1643
5	MS1196	Gordon A. Chandler	Org. 1677
5	MS1196	Gary W. Cooper	Org. 1677
1	MS0899	Technical Library (electronic File)	Org. 9536
1	MS0123	D. Chavez, LDRD Office	Org. 1011

FIGURE CAPTIONS

Figure 1. Schematic side view of baseline self-field axial gap ion diode (positive polarity)

Figure 2. Comparison of electron flow (from PIC simulations) in IVA geometry in negative polarity vs positive polarity, showing 'layered flow' in the latter.

Figure 3. Plot of the anode current I_A as a function of the cathode current I_C for equilibrium MITL flow at various voltages. Z_O is the vacuum impedance of the line. The scaling factor g(V) in Eq. 1 is included (from Ref. 22). The location of self-limited and minimum-current flow are also indicated.

Figure 4. Schematic drawing of Hermes load region showing location of various current monitors located on both inner and outer conductors.

Figure 5. Close-up of the diode region shown in Fig. 4.

Figure 6. Photograph, Fcup and peppershaker array after a beam experiment.

Figure 7. Exploded view of Ion Pinhole Camera.

Figure 8. Energy deposition profiles for radiochromic film as function of number of layers and incident proton energy.

Figure 9. Spall fluence threshold for aluminum and stainless steel as a function of proton energy.

Figure 10. Photograph of witness plate assembly with beamlet locating rods inserted.

Figure 11. Schematic view of the load region hardware used in radial diode experiments in positive polarity.

Figure 12. Schematic view, radial diode geometry used for negative polarity operation.

Figure 13. V(t) trajectory of Shots 8287 and 8493 projected onto $Z_oI_a - Z_oI_c$ space (Figure 3).

Figure 14. Scaling of load impedance and estimated diode voltage with ln $[r_{outer}/r_{inner}]$, for both positive and negative polarity radial diode shots.

Figure 15. a. Photograph, head-on view, stainless steel witness plate after Shot 8802. b. Side view of witness plate assembly with beamlet locating rods inserted after Shot 8802.

Figure 16. Photograph, aluminum witness plate front after Shot 8794.

Figure 17. Plot, waveforms, Shot 8794, including inner and outer currents, calculated non-saturated voltage, scaled Rogowski and Fcup signals.

Figure 18. a. Schematic layout of Fcup and peppershaker array prior to Shot 8524. b. Fcup waveforms, Shot 8524 (2), compared to Shot 8523.

Figure 19. Plot, waveforms, Shot 8842, including estimated voltage from nonsaturated calculation and from P-I-N diode unfold, inner and outer currents, and (scaled) Rogowski and (large) Fcup signals.

Figure 20. A. Photographs, a) shadowbox front before Shot 8839, b) after Shot 8839, and c) back of aluminum witness plate, after Shot 8839.

Figure 21. V(t) trajectory of Shots 8794 and 8844 projected onto Z_oI_a – Z_oI_c space (Figure 3).

Figure 22. V(t) trajectory of Shot 8841 onto Z_oI_a – Z_oI_c space (Figure 3).

Figure 23. V(t) trajectory of Shot 8957 projected onto Z_oI_a – Z_oI_c space (Figure 3).

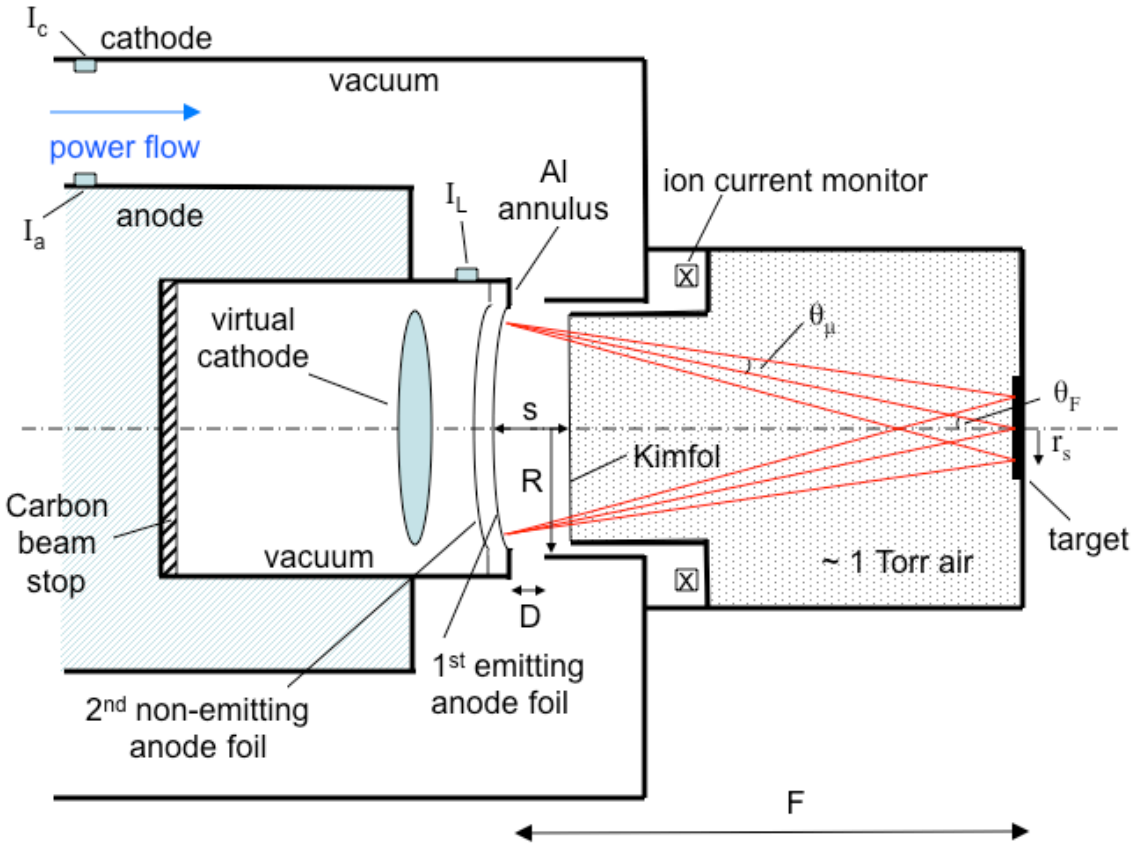
I_c
cathode
vacuum
power flow
I_a
anode
I_L
Al
annulus
ion current monitor
virtual
cathode
θ_μ
θ_F
s
r_s
Kimfol
R
Carbon
beam
stop
vacuum
~ 1 Torr air
target
D
1st emitting
anode foil
2nd non-emitting
anode foil
F

Fig. 1

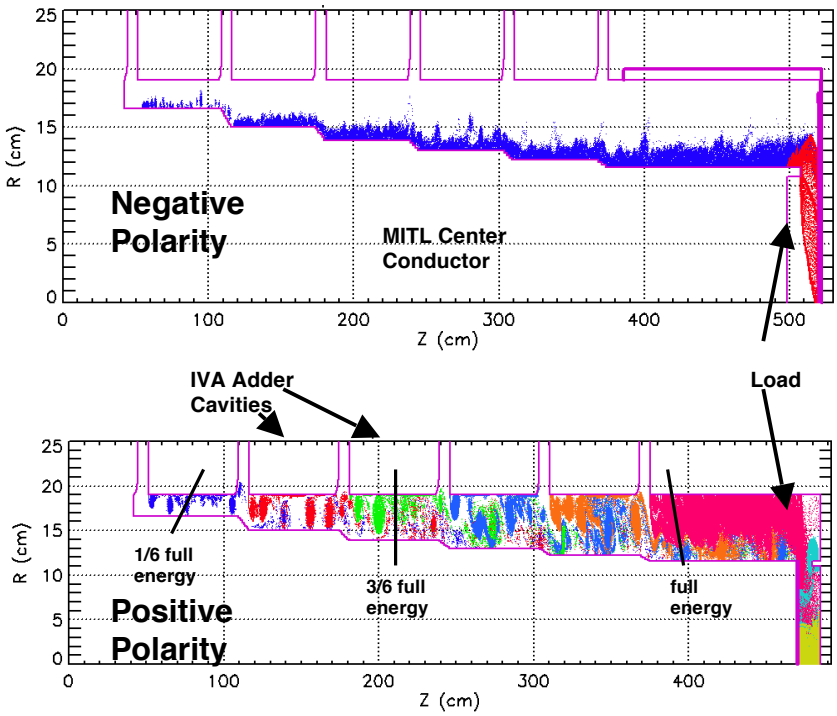
Negative
Polarity
MITL Center
Conductor
R (cm)
Z (cm)
IVA Adder
Cavities
Load
1/6 full
energy
3/6 full
energy
full
energy
Positive
Polarity
R (cm)
Z (cm)

Fig. 2

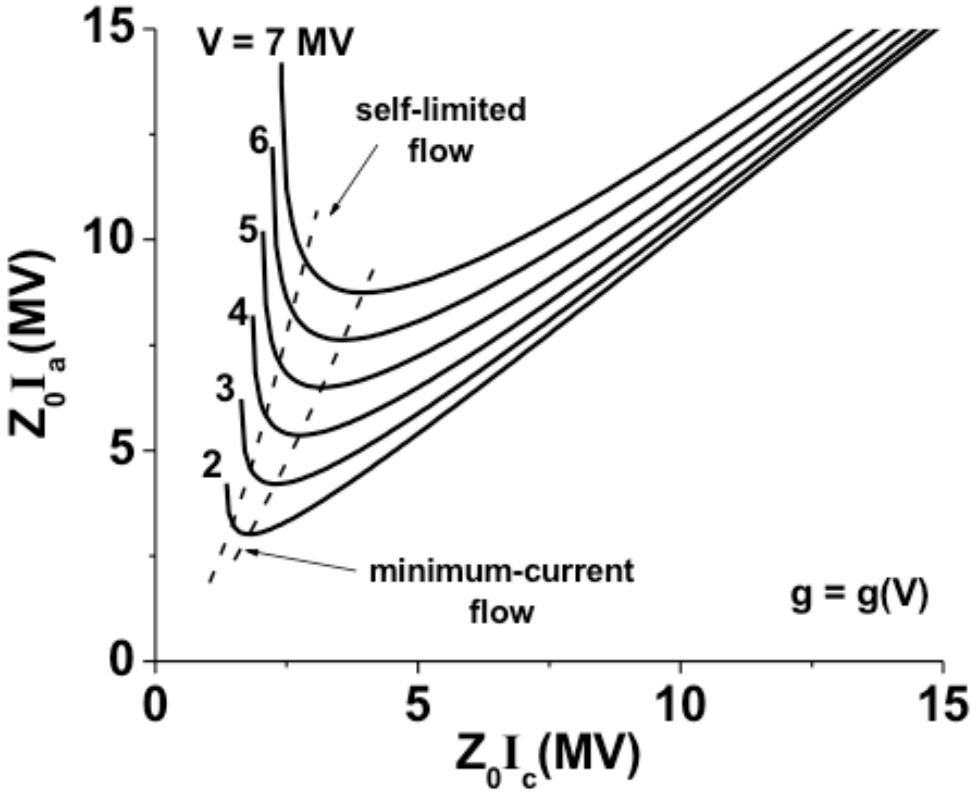
V = 7 MV
6
5
4
3
2
self-limited
flow
minimum-current
flow
g = g(V)
15
10
5
0
0
5
10
15
Z_0I_a(MV)
Z_0I_c(MV)

Fig. 3

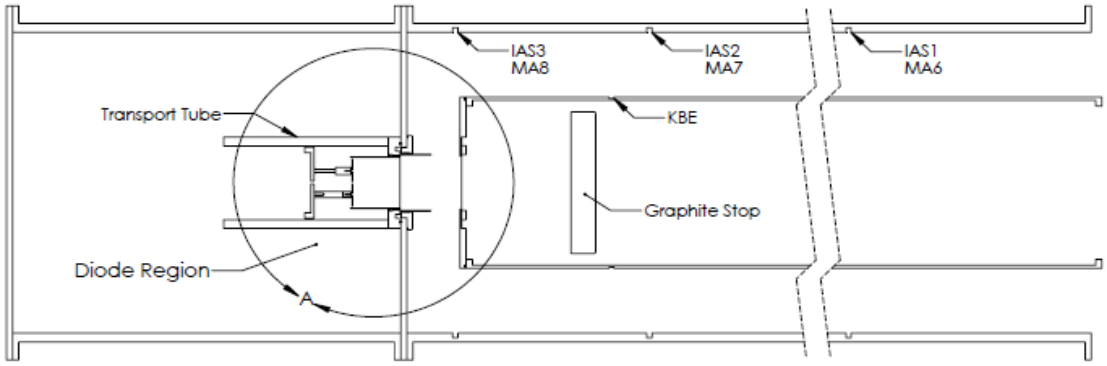
IAS3
MA8
IAS2
MA7
IAS1
MA6
Transport Tube
KBE
Graphite Stop
Diode Region
A

Fig. 4

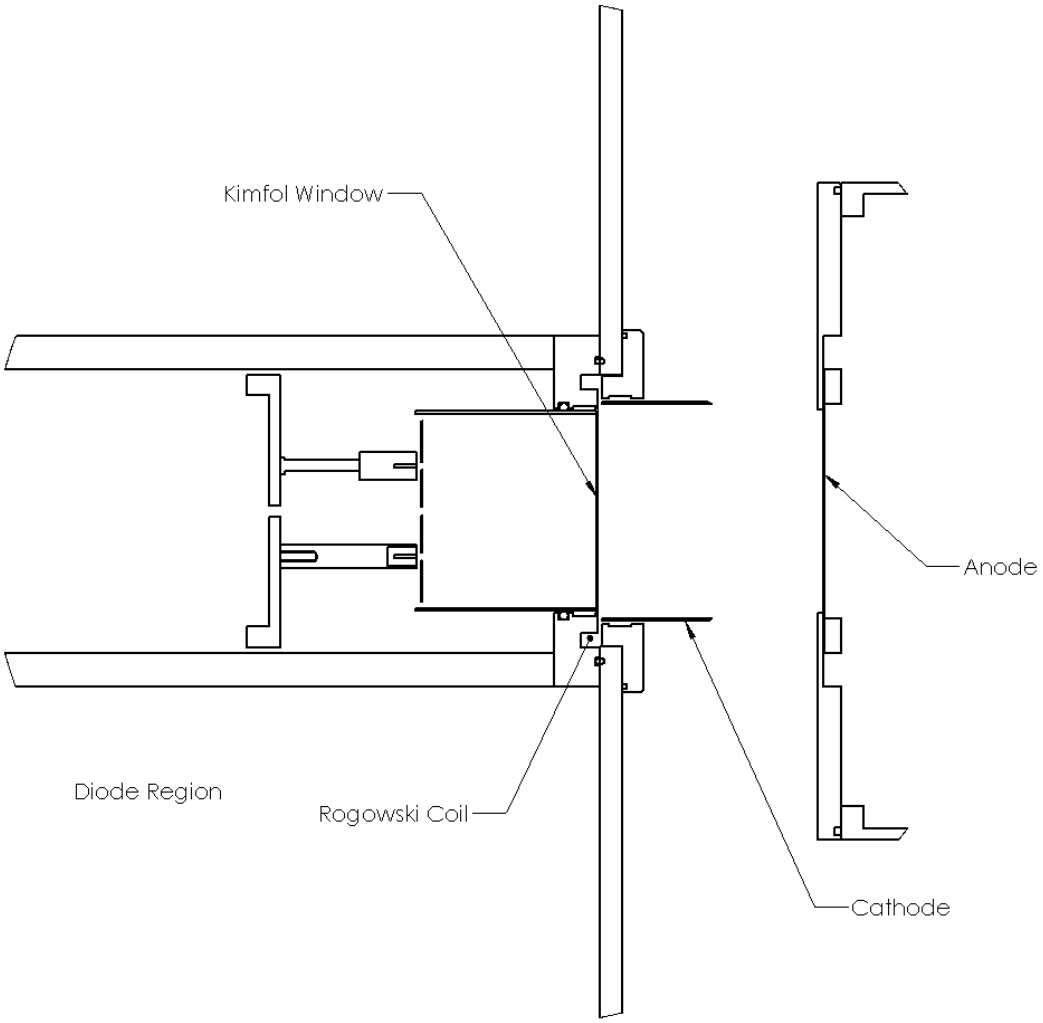

Fig. 5

Fig. 6

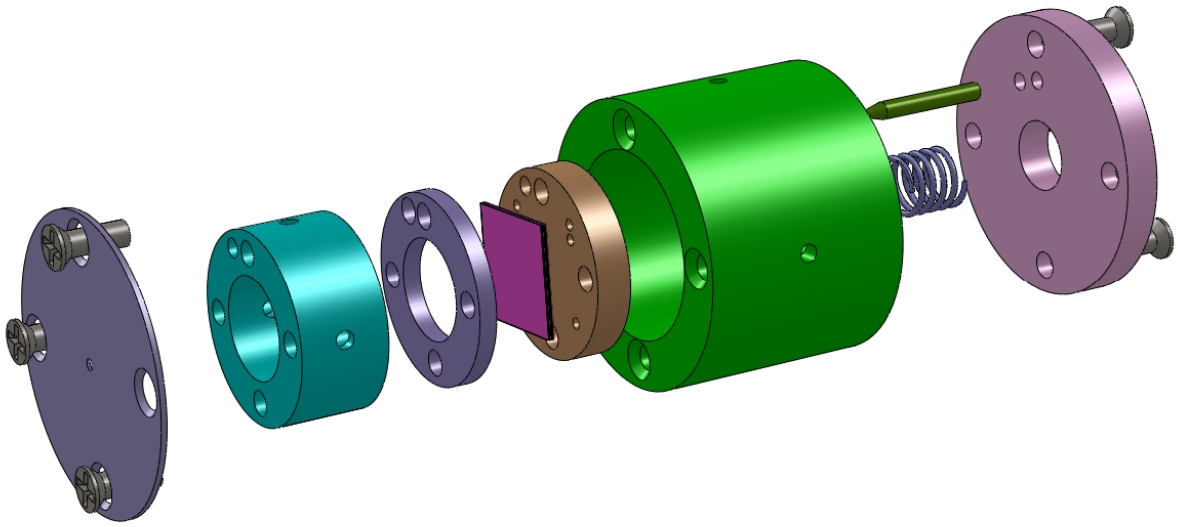

Fig. 7

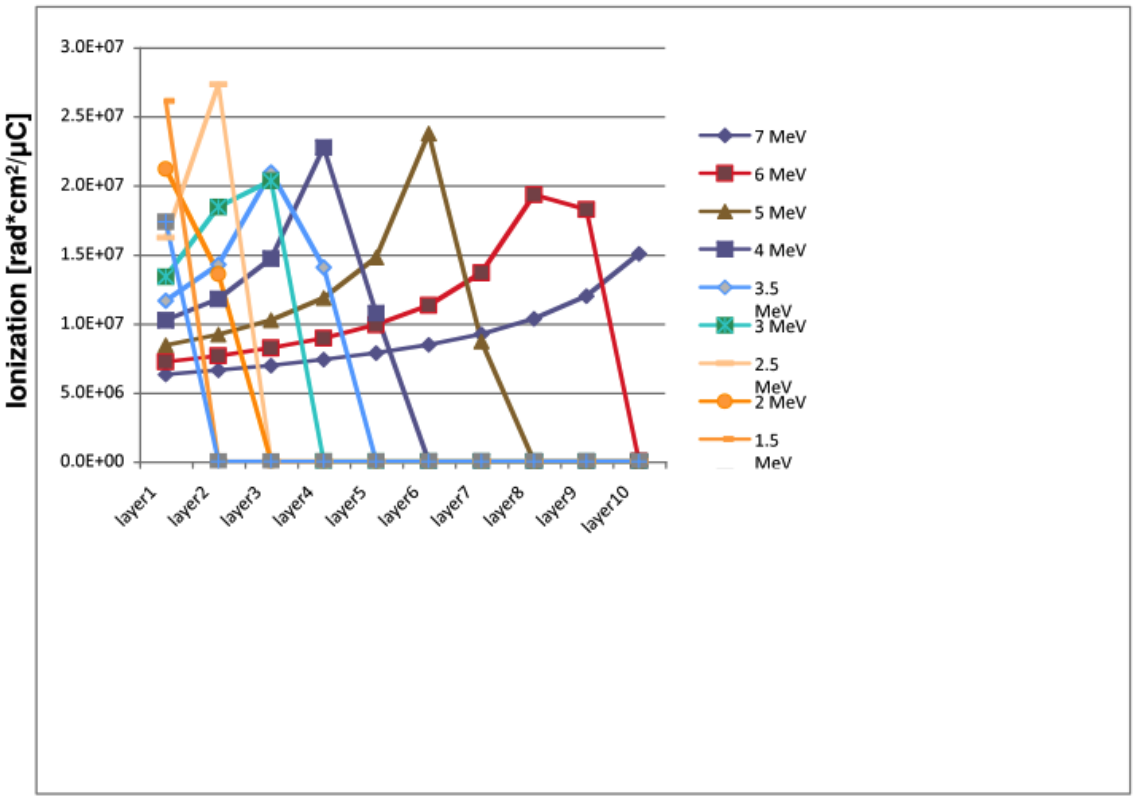
Ionization [rad*cm²/μC]
3.0E+07
2.5E+07
2.0E+07
1.5E+07
1.0E+07
5.0E+06
0.0E+00
layer1
layer2
layer3
layer4
layer5
layer6
layer7
layer8
layer9
layer10
7 MeV
6 MeV
5 MeV
4 MeV
3.5 MeV
3 MeV
2.5 MeV
2 MeV
1.5 MeV

Fig. 8

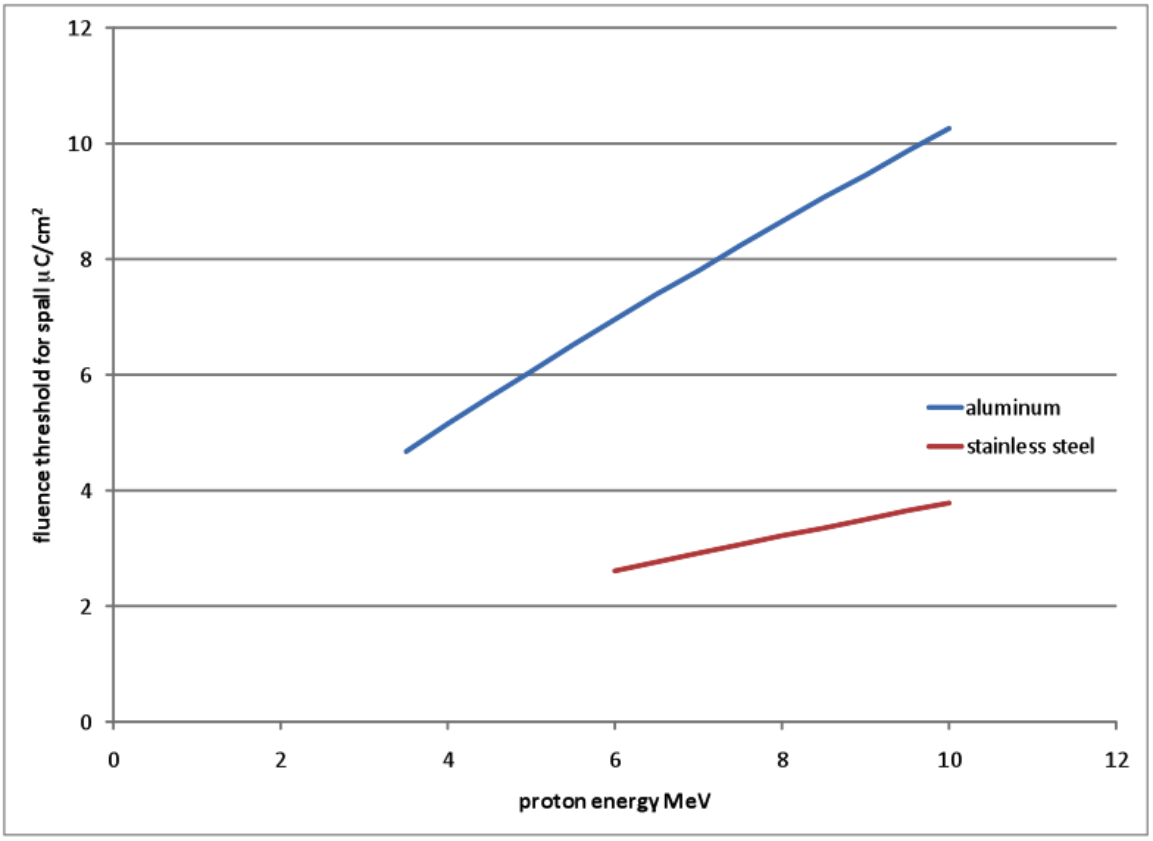
12
10
8
6
4
2
0
fluence threshold for spall μC/cm²
0
2
4
6
8
10
12
proton energy MeV
aluminum
stainless steel

Fig. 9

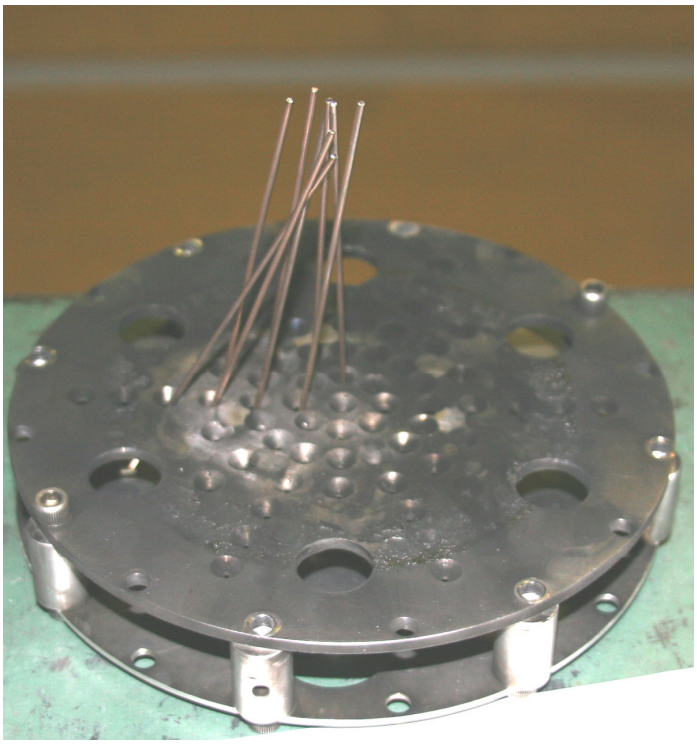

Fig. 10

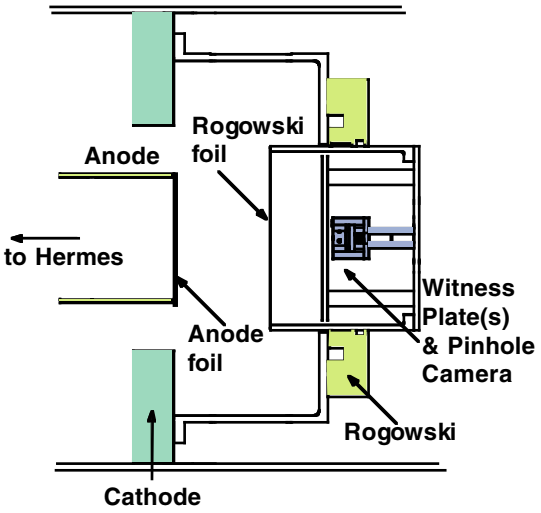
Rogowski
foil
Anode
to Hermes
Anode
foil
Witness
Plate(s)
& Pinhole
Camera
Rogowski
Cathode

Fig. 11

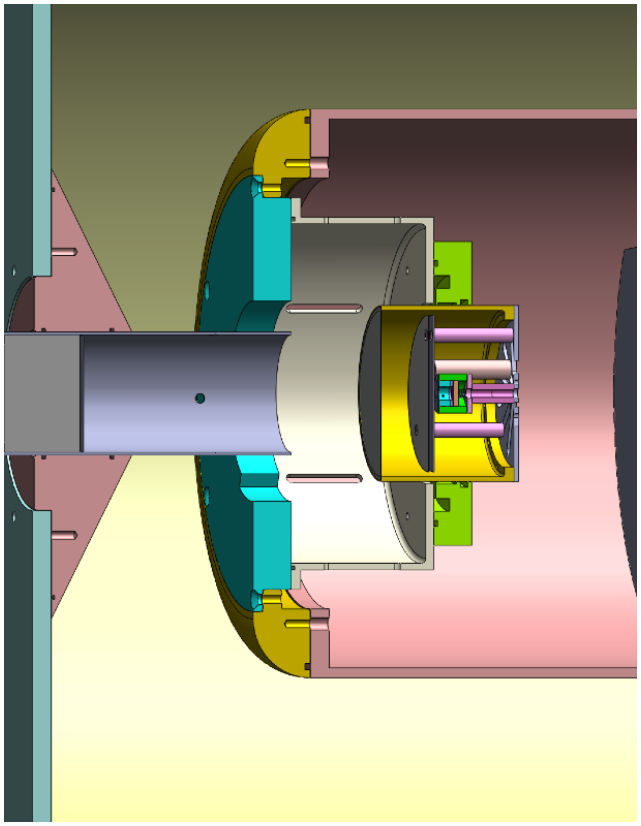

Fig. 12

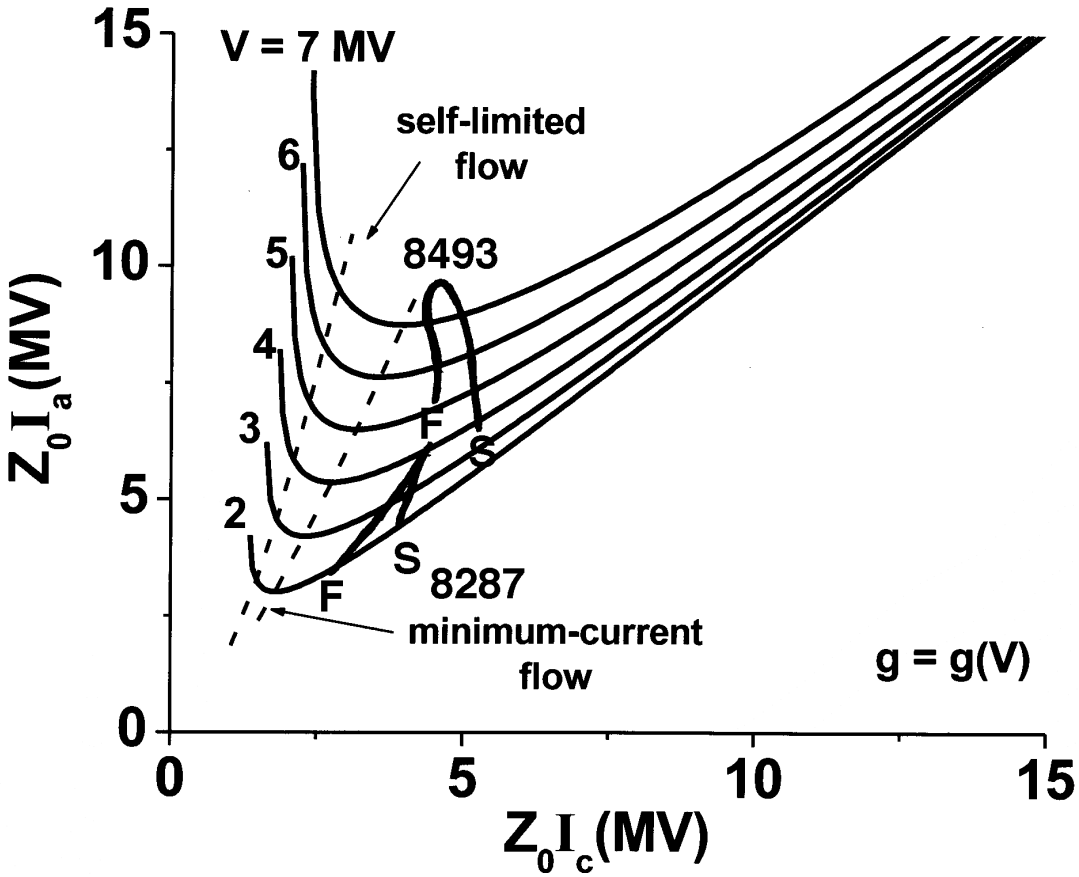
V = 7 MV
self-limited
flow
6
5
4
3
2
8493
F
S
S
8287
F
minimum-current
flow
g = g(V)
15
10
5
0
0
5
10
15
Z_0I_a(MV)
Z_0I_c(MV)

Fig. 13

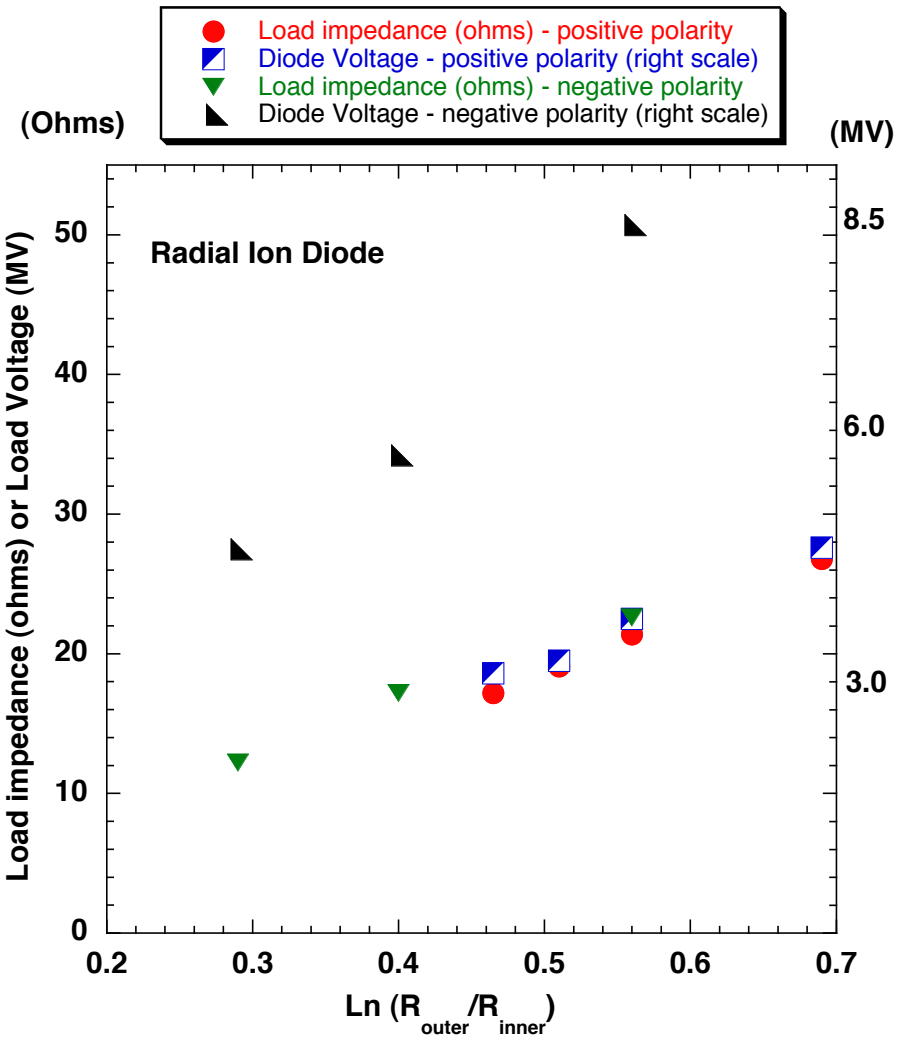
Load impedance (ohms) - positive polarity
Diode Voltage - positive polarity (right scale)
Load impedance (ohms) - negative polarity
Diode Voltage - negative polarity (right scale)
(Ohms)
(MV)
Radial Ion Diode
Load impedance (ohms) or Load Voltage (MV)
0
10
20
30
40
50
3.0
6.0
8.5
0.2
0.3
0.4
0.5
0.6
0.7
Ln (R outer /R inner)

Fig. 14

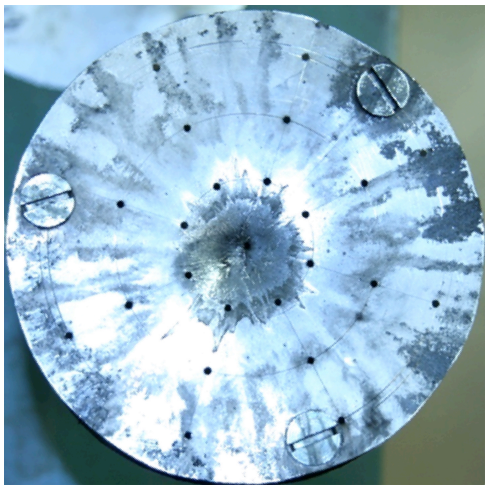

Fig. 15a

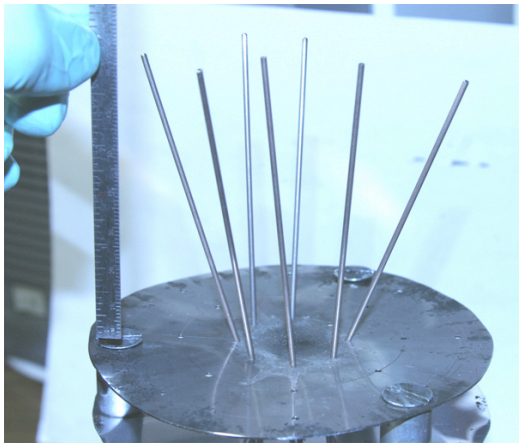

Fig. 15b

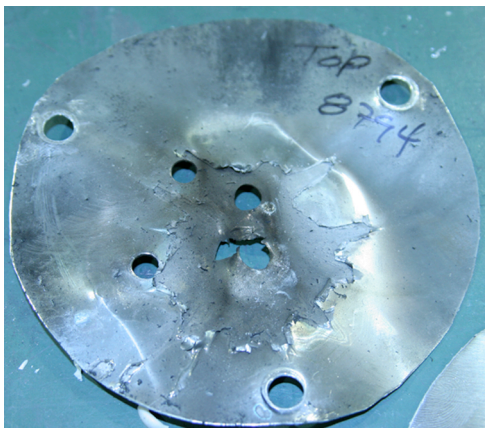

Fig. 16

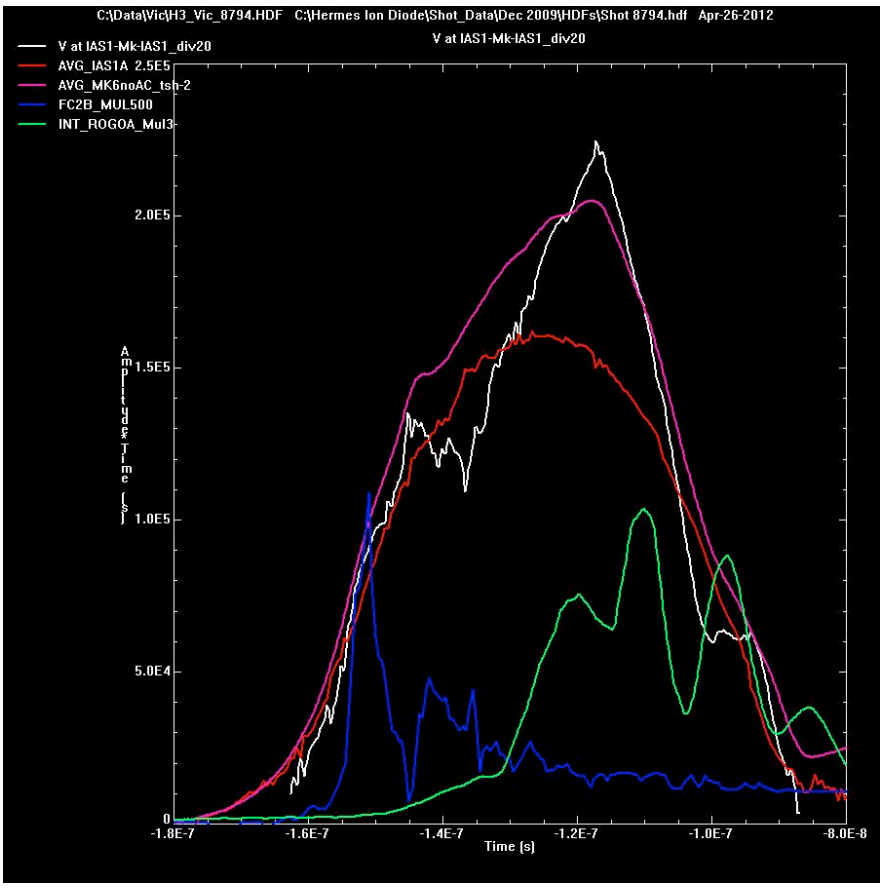
C:\Data\Vic\H3_Vic_8794.HDF C:\Hermes Ion Diode\Shot_Data\Dec 2009\HDFs\Shot 8794.hdf Apr-26-2012
V at IAS1-Mk-IAS1_div20
V at IAS1-Mk-IAS1_div20
AVG_IAS1A 2.5E5
AVG_MK6noAC_tsh-2
FC2B_MUL500
INT_ROGOA_Mul3-
2.0E5
1.5E5
1.0E5
5.0E4
0
Amplitude [Time [s]]
-1.8E-7
-1.6E-7
-1.4E-7
-1.2E-7
-1.0E-7
-8.0E-8
Time [s]

Fig. 17

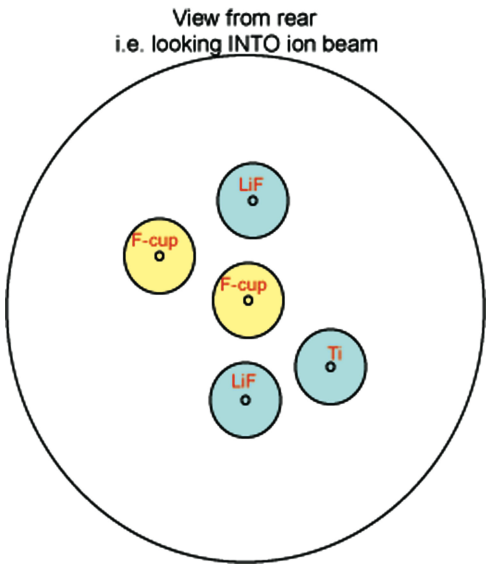

Fig. 18a

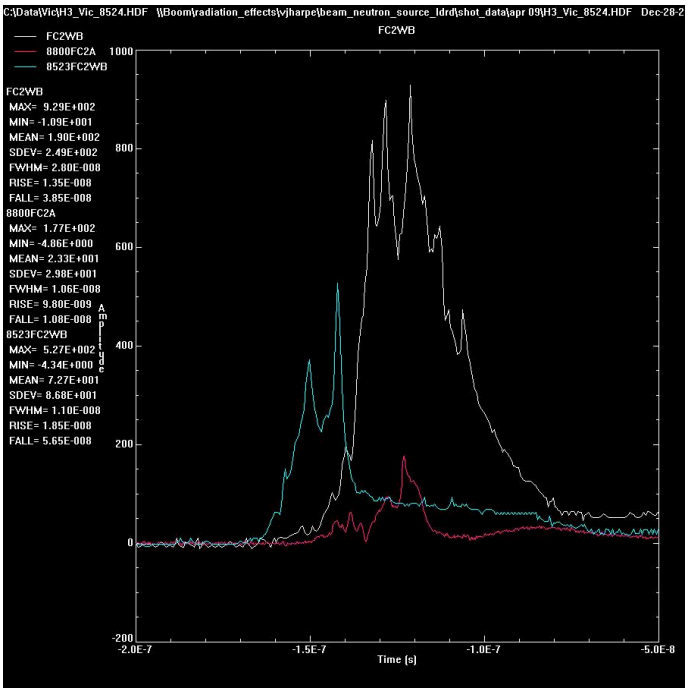

Fig. 18b

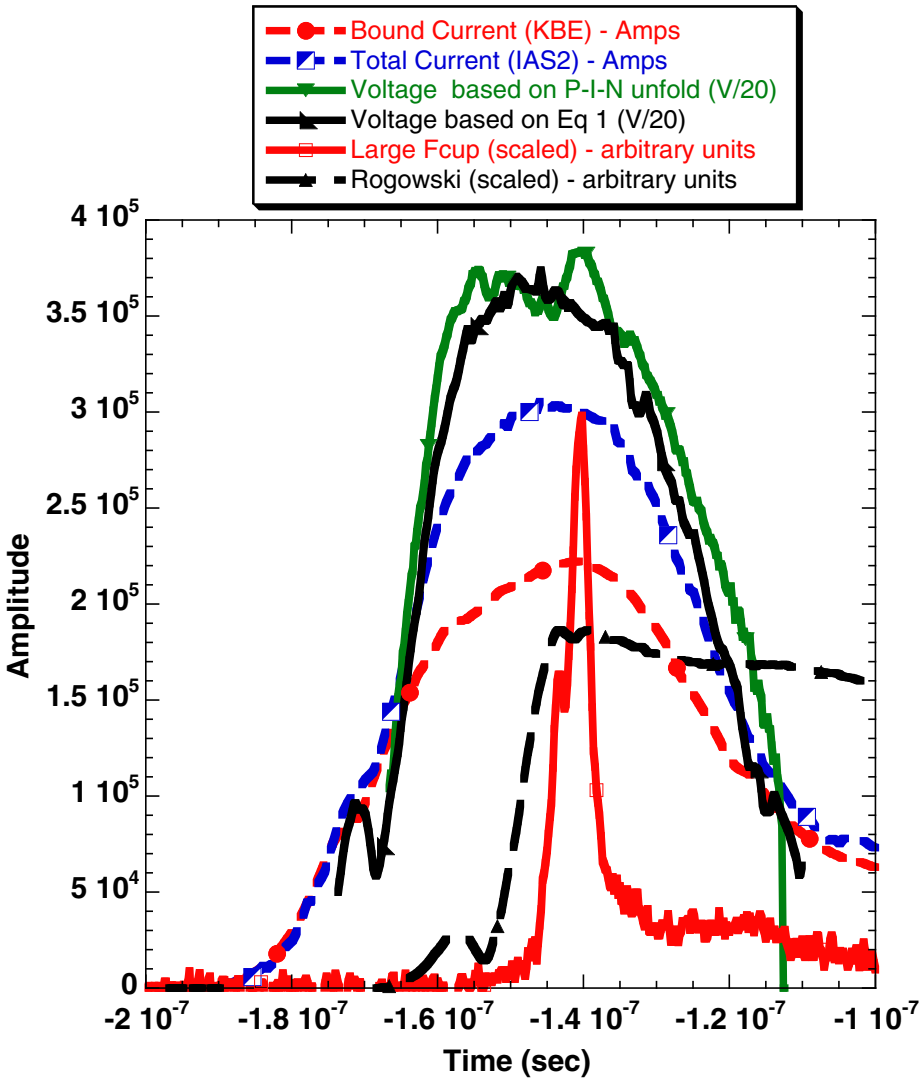
Bound Current (KBE) - Amps
Total Current (IAS2) - Amps
Voltage based on P-I-N unfold (V/20)
Voltage based on Eq 1 (V/20)
Large Fcup (scaled) - arbitrary units
Rogowski (scaled) - arbitrary units
Amplitude
Time (sec)
4 10^5
3.5 10^5
3 10^5
2.5 10^5
2 10^5
1.5 10^5
1 10^5
5 10^4
0
-2 10^-7
-1.8 10^-7
-1.6 10^-7
-1.4 10^-7
-1.2 10^-7
-1 10^-7

Fig. 19

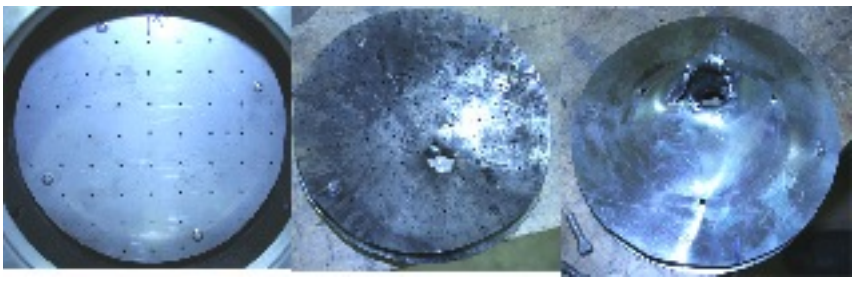

(a) (b) (c)

Fig. 20

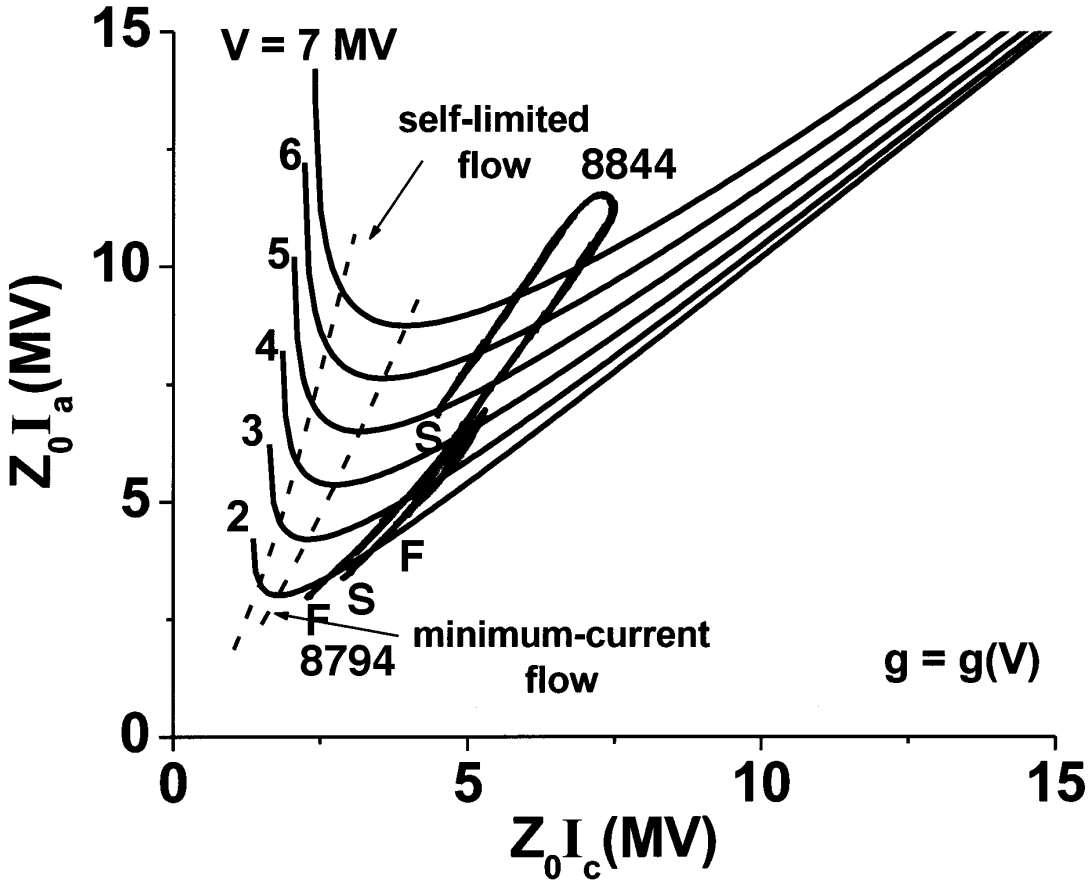
V = 7 MV
self-limited
flow
8844
6
5
4
3
2
S
F
S
F
8794
minimum-current
flow
g = g(V)
15
10
5
0
0
5
10
15
Z_0I_a(MV)
Z_0I_c(MV)

Fig. 21

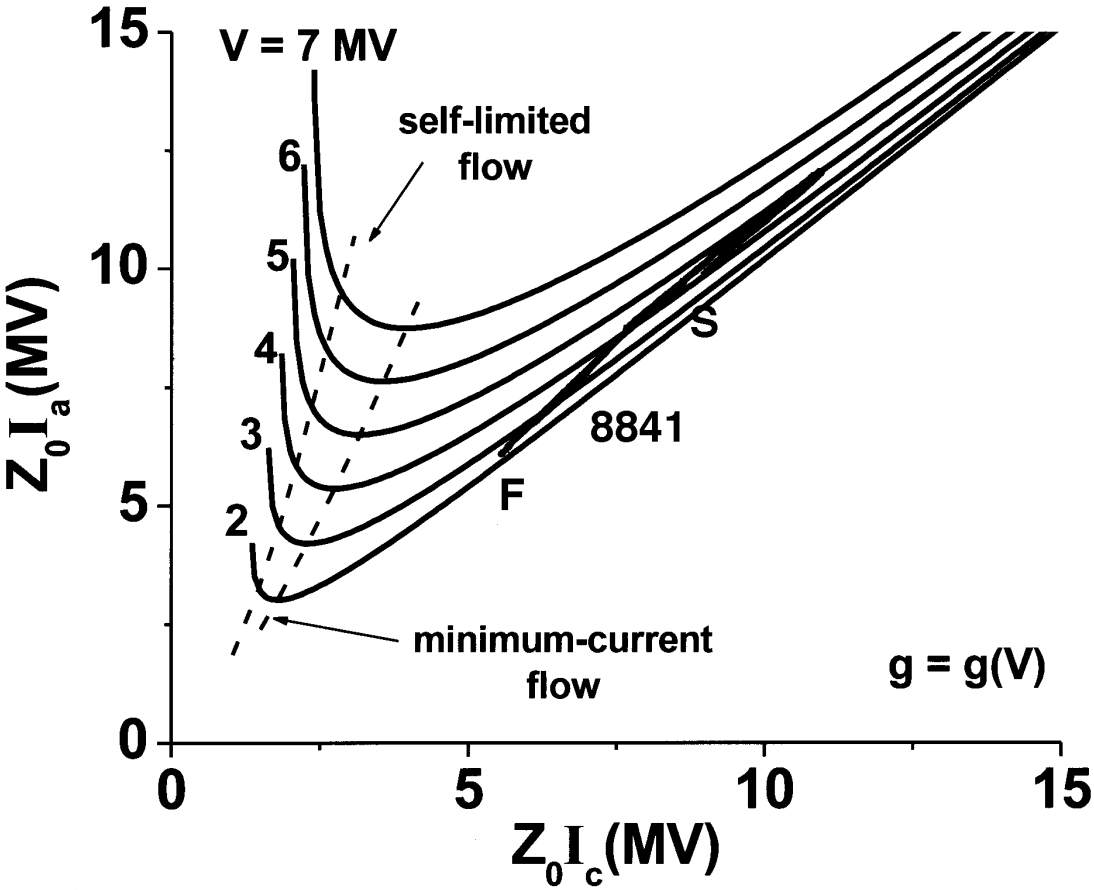
V = 7 MV
self-limited
flow
6
5
4
3
2
S
8841
F
minimum-current
flow
g = g(V)
Z_0I_a(MV)
Z_0I_c(MV)
0
5
10
15

Fig. 22

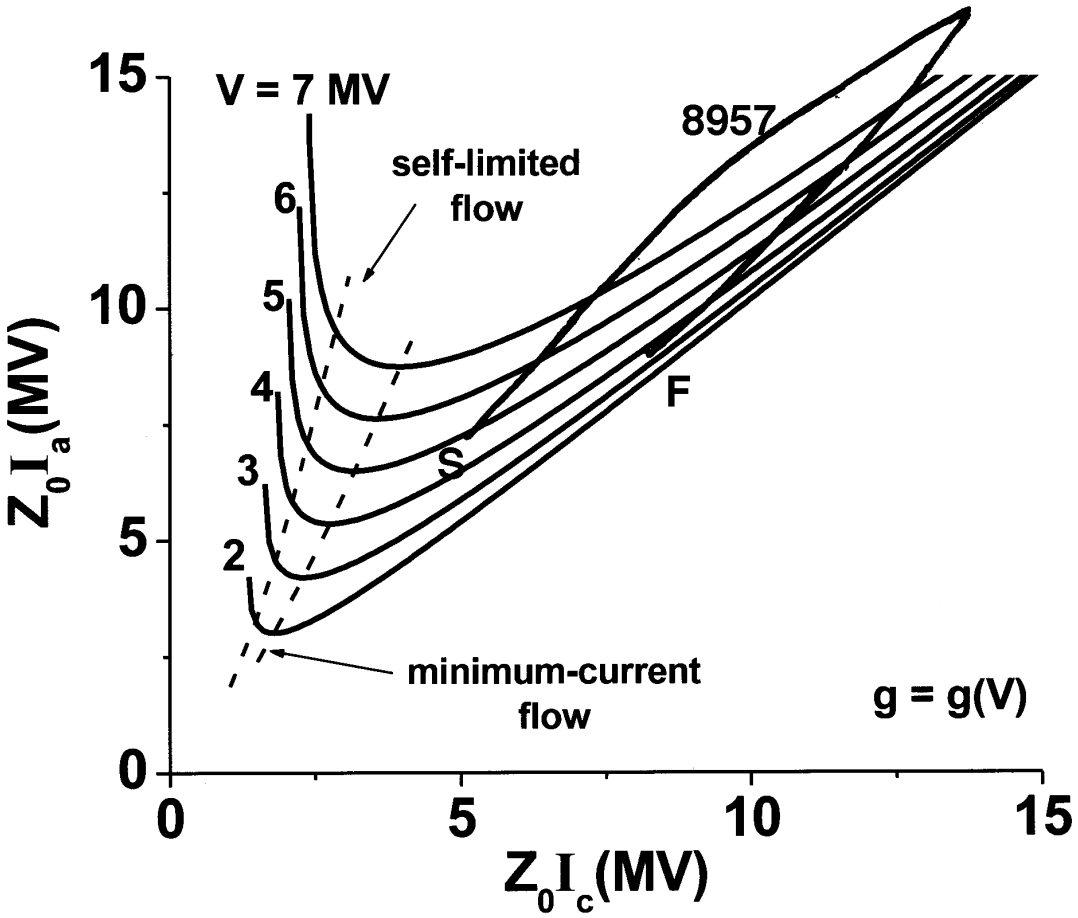
V = 7 MV
6
5
4
3
2
8957
self-limited
flow
S
F
minimum-current
flow
g = g(V)
15
10
5
0
0
5
10
15
Z_0I_a(MV)
Z_0I_c(MV)

Fig. 23